Published in final edited form as:
Dev Neurobiol. 2014 September ; 74(9): 851–876. doi:10.1002/dneu.22167.

Retinal Regeneration is Facilitated by the Presence of Surviving Neurons

Tshering Sherpa[1,2], **Tyler Lankford**, **Tim E. McGinn**[1,2], **Samuel S. Hunter**[1,3], **Ruth A. Frey**[1], **Chi Sun**[1,2], **Mariel Ryan**[1], **Barrie D. Robison**[1,2,3], and **Deborah L. Stenkamp**[1,2,3]

[1]Department of Biological Sciences, University of Idaho, Moscow, Idaho

[2]Graduate Program in Neuroscience, University of Idaho, Moscow, Idaho

[3]Graduate Program in Bioinformatics and Computational Biology, University of Idaho, Moscow, Idaho

Abstract

Teleost fish regenerate their retinas after damage, in contrast to mammals. In zebrafish subjected to an extensive ouabain-induced lesion that destroys all neurons and spares Müller glia, functional recovery and restoration of normal optic nerve head (ONH) diameter take place at 100 days post-injury. Subsequently, regenerated retinas overproduce cells in the retinal ganglion cell (RGC) layer, and the ONH becomes enlarged. Here we test the hypothesis that a selective injury, which spares photoreceptors and Müller glia, results in faster functional recovery and fewer long-term histological abnormalities. Following this selective retinal damage, recovery of visual function required 60 days, consistent with this hypothesis. In contrast to extensively damaged retinas, selectively damaged retinas showed fewer histological errors and did not overproduce neurons. Extensively damaged retinas had RGC axons that were delayed in pathfinding to the ONH, and showed misrouted axons within the ONH, suggesting that delayed functional recovery following an extensive lesion is related to defects in RGC axons exiting the eye and/or reaching their central targets. The *atoh7*, *fgf8a*, *shha*, and *netrin-1* genes were differentially expressed, and the distribution of Hh protein was disrupted following extensive damage as compared with selective damage. Confirming a role for Shh signaling in supporting rapid regeneration, $shha^{t4}$+/− zebrafish showed delayed functional recovery following selective damage. We suggest that surviving retinal neurons provide structural/molecular information to regenerating neurons, and that this patterning mechanism regulates factors such as Shh. These factors in turn control neuronal number, retinal lamination, and RGC axon pathfinding during retinal regeneration.

Keywords

retina; regeneration; zebrafish; photoreceptors; retinal ganglion cells; sonic hedgehog; optic nerve head; rosettes

Author for Correspondence: Deborah L. Stenkamp Department of Biological Sciences University of Idaho Moscow ID 83844-3051 Phone: 208-885-8963 Fax: 208-885-7905 dstenkam@uidaho.edu.

Introduction

Zebrafish have the ability to regenerate their retinas after damage. Following damage, Müller glia cells re-enter the cell cycle (Fimbel et al., 2007; Kassen et al., 2007; Yurco and Cameron, 2005) and produce multipotent neuronal progenitors (Nagashima et al., 2013), which can differentiate into all retinal cell types (Bernardos et al., 2007; Fausett and Goldman, 2006; Raymond et al., 2006). A number of specific factors have been identified as key regulators of this regenerative response to damage (Bailey et al., 2011; Lenkowski et al., 2013; Nagashima et al., 2013; Nelson et al., 2013; Qin et al., 2009; Ramachandran et al., 2011a; Ramachandran et al., 2010; Ramachandran et al., 2011b; Ramachandran et al., 2012; Thummel et al., 2011; Wan et al., 2012). This regenerative response is in contrast to the situation in humans and other mammals, where retinal damage usually results in a gliotic response, which includes hypertrophy of Müller glia and no production of new neurons. In some cases, however, mammalian Müller glia may re-enter the cell cycle, and under the appropriate conditions these glia have the capacity to become multipotent and generate retinal neurons (Karl et al., 2008; Ooto et al., 2004; Pollak et al., 2013; Ueki and Reh, 2013; Wan et al., 2008). There is therefore great interest in understanding the mechanisms and process of retinal regeneration in zebrafish, and applying this information toward the development and optimization of regenerative therapies for human retinal disorders (Fischer and Bongini, 2011; Stenkamp, 2011). For such therapies to be successful, however, new neurons must integrate into the damaged and potentially remodeled retina, and establish synaptic connections in a manner that restores function (Jones et al., 2012). Furthermore, regenerative therapies must be sufficiently controlled such that hyperplastic conditions do not arise. These latter issues are the focus of this paper.

Retinal regeneration studies in teleost fish demonstrate that regeneration of retinal neurons is possible after damage inflicted through surgical removal of retinal tissue (Cameron and Carney, 2000; Cameron and Easter, 1995; Hitchcock et al., 1992; Stenkamp and Cameron, 2002), light or laser induced photoreceptor ablation (Bernardos et al., 2007; Braisted et al., 1994; Meyers et al., 2012; Vihtelic and Hyde, 2000; Vihtelic et al., 2006; Wu et al., 2001), retinal puncture (Fausett and Goldman, 2006), genetic manipulations that target specific cell populations (Hochmann et al., 2012; Montgomery et al., 2011; Qin et al., 2011), or intraocular injection of the Na+/K+ ATPase inhibitor, ouabain (Fimbel et al., 2007; Maier and Wolburg, 1979; Nagashima et al., 2013; Negishi et al., 1988; Raymond et al., 1988; Sherpa et al., 2008). Intraocular ouabain injection is an especially interesting model for the following reasons. Adjustment of the ouabain concentration permits either widespread destruction of all retinal layers (Sherpa et al., 2008), or selective destruction of the ganglion cell layer (GCL) and inner nuclear layer (INL) (Fimbel et al., 2007), thereby targeting a region of the retina which cannot be selectively destroyed or damaged in other experimental paradigms. In addition, selective destruction of the GCL and INL via intraocular injection of a neurotoxin currently offers the only retinal degeneration/regeneration model with potential applications for the treatment of glaucoma, a retinal disorder in which RGCs die. Furthermore, because the damage is not localized to a specific region of the retinal hemisphere, ouabain injection also allows for the evaluation of loss and recovery of visual function using behavioral assays (Lindsey and Powers, 2007; Mensinger and Powers, 1999;

Sherpa et al., 2008) as important experimental endpoints for probing the ultimate success of the regeneration process.

A previous study from our laboratory (Sherpa et al., 2008) demonstrated that functional regeneration of zebrafish retina following extensive damage caused by high-dose intraocular injection of ouabain occurs in approximately 100 days. This corresponded to the amount of time required for the ONH to reach a size comparable to that of uninjected fish. However, at 100 days post-injury, the density of Islet-1+ neurons was higher in the regenerated samples than in the controls, suggesting abnormalities in neuronal production. In a separate study, in which the inner retinal layers of the zebrafish retina were selectively destroyed (Fimbel et al., 2007), there was no significant difference in the density of inner retinal neurons in regenerated retina as compared with undamaged control retinas. These data suggest that regeneration of retinal neurons may be regulated by the presence of other, undamaged, native retinal cells. Surviving cells may provide control of organizational cues and trophic factors, and/or may be involved in maintaining normal extracellular matrix configurations, facilitating the functional integration of new cells into the retina.

The current study has two goals. The first goal is to determine whether a lesion that spares photoreceptors results in faster visual recovery and fewer long-term histological errors. The second goal is to identify molecular factors that facilitate functional recovery. Our results support the hypothesis that functional recovery is faster, and long term histological outcomes are optimized, following selective damage that spares a population of neurons as well as Müller glia, as compared with extensive retinal damage that spares only the Müller glia. Furthermore, several genes involved in RGC development were differentially expressed following extensive vs. selective retinal damage, and defects in Shh signaling resulted in delayed functional recovery.

Methods

Animals and intraocular injections

Animals—Adult zebrafish (*Danio rerio)* of 6–12 months in age and approximately 3 cm total body length were maintained and bred in-house according to Westerfield (Westerfield, 2000) on a 14:10 h L/D cycle at 28.5 °C in aquatic housing units using recirculating system water. Most experiments were performed using a zebrafish strain originally purchased from Scientific Hatcheries (SciH; now Aquatica Tropicals; Plant City, FL) and currently maintained in-house. The *shh*^{t4}+/− zebrafish, their *shh*+/+ siblings, and the *GFAP:GFP* fish (Bernardos and Raymond, 2006) were propagated in-house from stock originally purchased from the Zebrafish International Resource Center (ZIRC; Eugene, OR). The *gap43:GFP* fish (Udvadia, 2008) were propagated in-house from embryos generously provided by Ava Udvadia (U. Wisconsin, Milwaukee). All procedures were approved by the Animal Care and Use Committee of the University of Idaho.

Ouabain Injections—Zebrafish were anaesthetized using buffered tricaine methanesulphonate (MS-222; Sigma, St. Louis, MO) (Westerfield, 2000). Intravitreal injections of ouabain (Sigma) were carried out as previously described (Fimbel et al., 2007; Nagashima et al., 2013; Sherpa et al., 2008). Selective retinal damage was achieved using

0.3–0.5 μL of 40 μM ouabain, resulting in an estimated intraocular concentration of 2 μM, and extensive retinal damage was achieved using the same volumes of 200 μM ouabain, resulting in an estimated intraocular concentration of 10 μM. With the exception of a set of experiments related to visual behavior (described in the next section), left (control) eyes were not injected.

Behavioral assays

Dorsal light reflex (DLR)—The dorsal light reflex (DLR) assay was performed to test the visual function of regenerating retina after selective damage; the procedure is similar to that described previously (Sherpa et al., 2008). Fourteen adult SciH zebrafish were injected intraocularly into the right eye with 2 μM ouabain to create unilateral selective retinal damage. In a separate experiment, a family of four *shha*^{t4}+/− fish and six *shha*+/+ siblings were similarly treated. The DLR maintains body axis orientation, using downwelling light as the environmental cue (Silver, 1974). Loss of visual function in one eye causes the fish to tilt such that the damaged eye "looks" upward (Mensinger and Powers, 1999). Fish were closely monitored daily by two independent and naïve observers who recorded normal or tilted orientation.

Place Preference Test—In separate experiments, a place preference test was performed to assay visual function. In captivity, zebrafish typically respond to an approaching person by moving toward the front of their tank and waiting under the feeding hole (Benner et al., 2010; Oswald and Robison, 2008; Sherpa et al., 2011). We recorded position of fish within a tank, following the waving of a hand (the visual stimulus) in front of the tank. Six bilaterally ouabain-injected fish and six uninjected control fish were maintained individually in one-liter tanks. Fish were randomly assigned to tanks and observers were naïve to the condition of the fish. Behavioral data were collected three times per day, and 3 days per week for 10 weeks. At each observation time, the vertical and horizontal locations of each fish were recorded three times over 3–5 seconds. Vertical location was coded with an integer (1–6, where 1 = top, 6 = bottom); horizontal location was recorded as a binary variable (1 = front half of the tank, 0 = back half of the tank) and these data were then used to calculate an approximate distance from the feeding area. A linear mixed effects model was fit in order to estimate average distance from feeding area and to test whether this distance was significantly different between control and injected fish for each observation time.

Histological methods

Retinal Cryosections—Fish were anesthetized, the cervical spinal cord was transected and the eyes were removed. Corneas were punctured with a microscalpel and eyes were fixed using 4% paraformaldehyde in phosphate-buffered 5% sucrose for 30 min. Lenses were removed, eyes were fixed an additional 30 min, and were then washed with increasing concentrations of phosphate-buffered sucrose prior to cryoprotection in 20% sucrose overnight at 4°C. The tissue was then embedded in a 1:2 mixture of OCT embedding medium (Sakura Finetek, Torrance, CA): 20% sucrose and then sectioned at 5–8 μm on a cryostat. As in our previous study (Sherpa et al., 2008), for all subsequent analyses, only central retinal regions were considered, to ensure that regeneration, rather than enhanced growth at the retinal margin (Stenkamp et al., 2001), was monitored.

Measurement of optic nerve heads (ONHs)—ONHs were measured as described previously (Fimbel et al., 2007; Sherpa et al., 2008; Sherpa et al., 2011). Briefly, three sections from each eye, containing the ONH, were stained with 0.1% methylene blue and brightfield images were collected. Scion Image/Fiji software (Schindelin et al., 2012) was used to measure the diameter of the ONH (Sherpa et al., 2008; Sherpa et al., 2011). For each section, the averages of three replicate measurements of ONH diameter were recorded.

Retinal whole mounts and confocal microscopy—Eyes were removed from dark-adapted, anaesthetized, sacrificed *gap43:GFP* fish, and submerged in PBS. A slit was cut in the cornea and the lens was removed. Whole retinas were peeled away from the RPE with fine forceps, were fixed in 4% paraformaldehyde in phosphate buffered 5% sucrose for 1 hr, and were then washed with buffered 5% sucrose, and then with phosphate-buffered saline (PBS). Retinas were cut in incomplete quadrants, mounted in Flouromount-G (Southern Biotech) with the RGC side up, and were imaged with an Olympus FV1000 confocal microscope. Confocal stacks were collected to capture the entire depth of all GFP+ processes, using a 20X (NA 0.75) objective. Projections of these stacks were rendered in Metamorph (version 7.7.0.0). GFP+ axon bundles were traced in Fiji using the Simple Neurite Tracer Plugin (Longair et al., 2011). Sholl analysis, typically used to analyze dendritic tree morphology (Kutzing et al., 2010) was used in the present study to analyze patterns of GFP+ axon bundles on projected image stacks. This analysis was carried out in Fiji with the Sholl Analysis Plugin using the semi-log method with 1 μm steps, excluding a 10 μm radius around the center of the ONH. The center of the ONH was identified by visual inspection of a corresponding brightfield image.

Immunocytochemistry—Retinal cryosections from zebrafish sacrificed at selected recovery times following damage were blocked in 20% normal goat serum, and then incubated with one of the following antibodies: anti-HuC/D (1:100, mouse monoclonal) (Molecular Probes, Eugene, OR); zpr-1 (1:200; mouse monoclonal), zrf-1 (1:200; mouse monoclonal), or zn8 (1:10; mouse monoclonal), all from ZIRC; anti-islet1 (1:200; mouse monoclonal) (Developmental Studies Hybridoma Bank, Iowa City, IA), anti-protein kinase Cα (1:200; rabbit polyclonal) (Santa Cruz); anti-PCNA (1:200, mouse monoclonal) (Sigma), anti-GFP (1:400; rabbit polyclonal) (Torrey Pines Biolabs, Secaucus, NJ), or anti-Shh (1:100, rabbit polyclonal) (AnaSpec, Fremont, CA; #55574). Blocked sections were incubated with primary antibody overnight at 4°C, washed in PBS containing 0.5% Triton X-100 (PBST), then incubated for 2 hours at room temperature with a Cy3-conjugated secondary antibody, donkey or goat anti-mouse (1:200) (Jackson Immunoresearch, West Grove, PA). Tissues were then washed in PBST, mounted in Vectashield containing the nuclear stain DAPI (Vector Laboratories, Burlingame, Ca) and imaged under epifluorescence optics with an upright Leica DMR microscope (Bartels and Stout, Issaquah, WA). For the set of experiments utilizing the *GFAP:GFP* transgenic line, antigen retrieval (of PCNA) was carried out by incubating sections for 10 mins at 98°C in 10 mM sodium citrate (pH 6.0) containing 0.05% Tween20, then rinsing sections in PBS for 10 min at room temperature. Some of these sections were imaged with the Leica DMR, and others with the Olympus FV1000 confocal microscope, using a 60x (oil immersion; NA 1.42) objective.

Western blotting—Wild-type (SciH) zebrafish embryos, 24–30 hpf, were dechorionated manually with forceps, and de-yolked by trituration. Fifty embryos were collected in 200 μL extraction buffer containing 0.5% SDS, 0.5% sodium deoxycholate, 2μg/mL aprotinin, 2 μg/mL leupeptin, 1 μg/mL pepstatin A, and EDTA-free protease inhibitor cocktail (one tablet/7 mL; Roche Diagnostics, Indianapolis, IN) in PBS. After homogenization, 100 μL phenylmethylsulfonyl fluoride (1.3 mg/mL in 100% ethanol) was added to the tissue mixture, which was then incubated on ice for 30 min. Samples were centrifuged 13,000 rpm at 4°C for 20 min, and 15 μL of the supernatant was loaded per well. Proteins were separated on a 10% polyacrylamide gel (70V for 100 min), and were transferred overnight (25V) to PVDF membranes. Membranes were blocked with 5% bovine serum albumin in TBST for one hr, and immunoblotted with anti-Shh at 1:1000 overnight. Membranes were then blotted with a horseradish peroxidaseconjugated secondary antibody (2 hrs, 1:3000; Jackson Immunoresearch), and detection was carried out with the Pierce ECL chemiluminescent Western blotting substrate (Thermo Scientific).

Neuronal cell counting—Three retinal cryosections per eye were immunolabeled with anti-HuC/D monoclonal antibody, to detect differentiated amacrine and ganglion cells (Fimbel et al., 2007; Sherpa et al., 2011; Stenkamp et al., 2008a). HuC/D-positive cells in the INL and GCL were counted on these sections over a distance of 110 μm. Total inner retinal neuron densities were calculated by dividing total cell counts by area (110 μm distance × 8 μm section thickness). Cell densities were compared across conditions using ANOVA followed by posthoc comparisons corrected for multiple testing using the multicomp (Hothorn et al., 2008) package in R (R Core Development Team, 2005).

Assessment of lamination and rosettes—Three sections per eye were stained with anti-HuC/D antibody and slides were mounted in Vectashield containing DAPI. The total curvilinear length of the retina was measured. The retina was then visually examined for regions in which there was not a clear distinction between INL and GCL (see Fig. 4 for examples). Lengths of these regions were then measured, summed, and divided by the total length of the retina in order to calculate the percentage of “laminar fusion” per section. The presence of rosettes was evaluated by immunohistochemistry using the zpr-1 marker for cone photoreceptors.

Quantitative analysis of gene expression

RNA preparation—After fish were anesthetized and sacrificed, total RNA was isolated from treated and control whole eyes using the RNeasy Mini Kit (Qiagen, Valencia, CA), followed by DNase treatment. RNA was quantified spectrophotometrically (Nanodrop 1000; ThermoScientific, Wilmington, DE). There were 4 biological replicates for each sampling time, and contralateral uninjected eyes, or eyes obtained from untreated fish, were used as controls.

Quantitative RT-PCR—Levels of *her4.2*, *shha*, *Brn3b*, *fgf8a*, *ptc-2a*, *ath5*, *KLF6a*, and *netrin* mRNA in control and regenerating retinas were quantified by quantitative real-time RT-PCR (qRT-PCR). First-strand cDNA was synthesized with 100 ng of total RNA, 100 ng random primers (Invitrogen, Carlsbad, CA), and 50 U reverse transcriptase (Superscript II;

Invitrogen), according to the manufacturer's protocol. qRT-PCR was performed (model 7900HT Fast Real-Time PCR System using SYBR-Green PCR Master Mix; AppliedBiosystems, Inc. [ABI], Foster City, CA) according to the manufacturer's protocol. cDNA was diluted 1:5 with TE (pH 8.0) and used as a template in the reactions. Specificity of the reactions was verified with melt-curve analysis. Four biological replicates and two technical replicates were performed for each tissue type. 18S rRNA was used as the endogenous reference gene. Before statistical analysis, CT values for both the target genes and the reference gene were averaged across technical replicates. All primers were designed using Primer Express 3.0 (Applied Biosystems) (Table 1).

Photography and statistics

Most images were collected using a SPOT camera and associated software (Diagnostic Instruments). Images in Fig. 3 and Supplemental Fig. 1 were collected using an Olympus FV1000 confocal microscope. In some cases, images obtained under different optical conditions were combined using the “apply image” function in Adobe PhotoshopCS1 or CS6. Statistics were performed in R (R Core Development Team, 2005), or with SASS.

Results

Selective retinal damage spares only photoreceptors, Müller glia, and rarely horizontal cells

Our previous behavioral studies demonstrated that zebrafish recover visual function at 98 days post injury (dpi) after an extensive retinal injury inflicted by intraocular exposure to 10 μM ouabain (Sherpa et al., 2008). We wished to utilize a comparative lesioning strategy to test the hypothesis that functional recovery may be faster following a more selective lesion that damages fewer cell types. To gain a better understanding of the specific cell types that survive extensive vs. selective retinal lesions and may influence the regenerative process, we evaluated the presence of photoreceptors, Müller glia, horizontal cells, and bipolar cells using specific markers, at the peak of ouabain-induced retinal cell death [3–4 dpi; (Fimbel et al., 2007; Sherpa et al., 2008)]. Selectively lesioned retinas showed zpr-1+ cone photoreceptors (Fig. 1A), and zrf-1+ (GFAP+) Müller glia (Fig. 1B). Photoreceptors had normal morphologies, but the glia displayed disorganized morphologies, and more brightly stained apical processes (compare to undamaged retina in Fig. 1H) [see also (Nagashima et al., 2013)]. Occasionally, selectively damaged retinas also showed islet1+ cells near the outer plexiform layer (Fig. 1C); these likely correspond to horizontal cells (Whitney et al., 2011). RGCs (HuC/D+; data not shown), and subsets of retinal bipolar cells (PKCα+; Fig. 1D), and amacrine cells (calbindin+; data not shown) only very rarely survived the selective lesion.

Extensively damaged retinas showed the sporadic presence of zpr-1+ photoreceptor debris (Fig. 1E), and zrf-1+ Müller glia with highly disorganized processes that invaded what was formerly the interphotoreceptor space (Fig. 1F). No other retinal cell markers (islet1, PKCα, data not shown) generated positive signals in extensively damaged retinas at 4 dpi. Within the neural retina, the extensive lesion therefore spares only Müller glia, while the selective

lesion spares Müller glia, photoreceptors, occasionally horizontal cells, and the very rare PKCα+ bipolar cell.

We also wished to determine whether the Müller glia spared by extensive retinal damage re-entered the cell cycle to participate in the regenerative process, as this has not been previously demonstrated for this mode of damage. Eyes of *GFAP:GFP* transgenic zebrafish (Bernardos and Raymond, 2006) were subjected to extensive ouabain damage, and were fixed at 4 dpi and processed as cryosections with an anti-PCNA antibody to label cells in S-phase. Epifluorescence microscopy revealed strips of retinal tissue that were almost completely GFP+, containing numerous clusters of PCNA+/DAPI+ nuclei (Fig. 1G). We carried out further imaging of these retinal sections using confocal microscopy, and verified that numerous PCNA+/DAPI+ nuclei were also GFP+ (Supplemental Fig. 1A–D). These findings suggest that, as in response to other forms of retinal damage in the zebrafish (Bernardos et al., 2007; Fausett and Goldman, 2006), Müller glia re-enter the cell cycle following a high-dose ouabain lesion that destroys all retinal neurons.

Finally, we wished to determine whether Müller glia engaged in increased Notch signaling in response to an extensive lesion, and so carried out quantitative RT-PCR (qRT-PCR) of the Notch signaling gene *her4.2* at several sampling times (1, 2, 3, 5, 6, 8, 12, and 20 dpi) after lesioning. *Her4.2* is upregulated in Müller glia (Qin et al., 2009) and in whole retina (Kassen et al., 2007) at 2 dpi following intense light lesions. In eyes subjected to selective damage, *her4.2* expression was upregulated at 6 and 8 days after ouabain injection, suggesting a delayed response as compared to the response to light damage (Supplemental Fig. 1E). Interestingly, in eyes subjected to extensive damage, *her4.2* expression was significantly ($p<0.01$) upregulated at 5, 6, 8, and 12 days after ouabain injection, suggesting a slightly more rapid and sustained response (Supplemental Fig. 1E). Collectively these findings document the immediate outcomes of selective vs. extensive lesioning processes and indicate that the initial proliferative responses of Müller glia are slightly more robust following extensive lesion.

Functional recovery of vision after selective damage to inner retinal neurons

To determine the time-course of functional recovery following a selective retinal injury that spares photoreceptors as well as Müller glia, we used two complementary behavioral assays: the dorsal light reflex (DLR) assay (Sherpa et al., 2008), and a place-preference assay (Sherpa et al., 2011). Fourteen fish were subjected to unilateral, intraocular injection of 2 μM ouabain, and the DLR was monitored during recovery. All fish tilted their dorsoventral body axes away from the injured eye within one day of injury, and all of them recovered and sustained a normal DLR at 60 dpi (data not shown). Another six fish were subjected to bilateral retinal damage, and a different, visually-mediated behavior was monitored during the retinal regeneration period, in comparison to that of five undamaged control fish. The place-preference assay used here is based upon the observation that captive, wild-type zebrafish respond to the sight of a human hand by approaching the tank's feeding hole, in anticipation of a meal (Benner et al., 2010; Oswald and Robison, 2008; Sherpa et al., 2011). Positions of treated fish within their individual tanks were significantly different from those of control fish over the first 60 days of the regeneration period [Fig. 2; $p<0.05$; Simultaneous

Tests for General Linear Hypotheses (Hothorn et al., 2008)]. At 61 dpi and beyond, however, there were no significant differences in place preference between ouabain-treated and control fish (Fig. 2). Therefore, selective damage that spares photoreceptors and Müller glia results in a regenerative response that is successful at restoring vision. The return of visual function (at 60–61 dpi; Fig. 2) occurs more rapidly than that following retinal damage that spares only Müller glia [at 98 dpi; (Sherpa et al., 2008)].

Delayed and abnormal intraocular pathfinding of RGC axons after extensive damage

Delayed restoration of ONH size following extensive but not selective lesion despite similar time-courses for generation of new RGCs ((Fimbel et al., 2007; Sherpa et al., 2008), and see below), suggests possible defects in RGC axon pathfinding to the ONH during regeneration after an extensive lesion. To test this hypothesis, we used the transgenic line *gap43:eGFP*, in which neurons with actively growing axons express eGFP under control the of Takifugu *growth-associated protein 43* (*gap43*) promoter (Udvadia, 2008). Eight fish were subjected to unilateral selective lesion, and eight fish were subjected to unilateral extensive lesion, and were sacrificed at 21 dpi, or at 53 dpi, a time when the ONH has nearly returned to normal size in the case of selectively lesioned retinas (Fimbel et al., 2007). The nerve fiber layer of flat-mounted retinas was subjected to confocal imaging (Fig. 3). Control (undamaged) retinas showed labeling of a small number of thin axon bundles originating from peripheral retina - where the most recently generated retinal neurons reside in an undamaged retina (Marcus et al., 1999) (Fig 3A). Selectively-lesioned retinas processed at 21 and 53 dpi showed many more strongly labeled axon bundles, suggesting an increase in the number of *gap43:GFP+* axons, and/or upregulation of the *gap43:GFP* transgene, reflecting active axon growth (Fig. 3B). Many of the axons were gathered into larger bundles than those seen in undamaged retinas, and the majority projected centrally – toward the ONH – consistent with successful RGC axon pathfinding within the eye. However, some samples contained axon bundles that crossed other bundles and bypassed the ONH (Fig. 3D'). Extensively damaged retinas processed at 21 and 53 dpi displayed greater variability in the apparent densities and trajectories of GFP+ axon bundles, and in general appeared more disorganized (Fig. 3C, E). In some cases large bundles of axons looped, meandered and crossed each other within the eye, particularly in 21 dpi samples (Fig. 3C), and many axon bundles did not reach the ONH (arrows in Fig. 3C). In other cases axon bundles were sparse and narrow (Fig. 3C') in contrast with those in selectively damaged retinas. However, extensively lesioned retinas sampled at 53 dpi showed more axon bundles than at 21 dpi, and displayed axon trajectories that more accurately reached the ONH (Fig. 3E).

To complement our qualitative findings we carried out Sholl analysis (Kutzing et al., 2010), by counting the number of axon bundle intersections with concentric circles of increasing radius (1 μM steps), centered at the ONH (see *s in Fig. 3A–E). Quantitative output of these analyses are shown in Figs. 3F–H, and Supplemental Fig. 2. The number of paths taken by axon bundles, and the maximum number of axon bundles, were each statistically indistinguishable in selectively damaged samples as compared with control retinas, but were significantly greater in 53 dpi extensively damaged retinas as compared with controls, and as compared with 21 dpi extensively damaged retinas (Fig. 3F, G; $p<0.05$, ANOVA with Bonferroni post-hoc analysis). These results suggest greater complexity of the axon patterns

in 53 dpi extensively lesioned retinas. The `critical value' (distance at which the maximum number of axon bundle intersections was measured) averaged approximately 200 to 250 μM, but with high variability in many of the experimental conditions (Fig. 3H). Semi-log plots derived from Sholl analysis (representative plots shown in Supplemental Fig. 2A) were used to determine regression coefficients (Sholl "k" values), as a measure of the change in density of axon bundles as a function of distance from the ONH (Kutzing et al., 2010). These values were remarkably similar across conditions, although at 21 dpi following an extensive lesion there was wide variability in k values (Supplemental Fig. 2B). We also compared the regression R^2 values, and these were statistically indistinguishable across conditions (Supplemental Fig. 1C; ANOVA). The results of the Sholl analysis indicate the extensively lesioned retinas display greater complexity in their RCG axon patterns at 53 dpi. Together with the qualitative findings our results support the hypothesis that RGC axon pathfinding to the ONH is delayed and abnormal following extensive as compared with selective retinal lesion.

Correction of histological errors following selective damage

Lamination errors have been reported in the regenerated retinas of teleost fish (Cameron and Carney, 2000; Hitchcock et al., 1992; Raymond et al., 1988; Stenkamp et al., 2001) as well as in the blind *lrp2* ("*bugeye*") mutant that engages in a proliferative response to ongoing neuronal stress (Sherpa et al., 2011). It is possible that failure to correct lamination defects may also underlie the delay in functional recovery in extensively vs. selectively damaged zebrafish retinas. In order to assess histological accuracy of regenerated zebrafish retina over a time frame that includes the restoration of visual function, we stained retinal cryosections with a combination of the neuronal marker anti-HuC/D, and the nuclear stain DAPI. Sections were inspected for the presence of "laminar fusions," in which neuronal cell bodies were positioned (abnormally) within the inner plexiform layer. Representative sections containing laminar fusions are shown in Figure 4. In some cases, particularly at early recovery times, these fusions were widespread, making for difficulty in distinguishing the GCL from the INL (Fig. 4A,E). In other cases, they were less severe, but were very regularly seen throughout the retina (Fig. 4B,F). In some of the sections processed at late recovery times (100 and 160 dpi) following extensive retinal damage, the lamination errors were even more severe and involved the entire thickness of the retina (Fig. 4G,H), while their counterparts processed following selective retinal damage showed comparatively fewer histological errors (Fig. 4C,D).

We measured the proportion of each retinal section containing laminar fusions (in three sections per eye, n=6 fish for each sampling time; see Methods). All of the retinal sections evaluated from damaged and regenerating retinas showed widespread laminar fusions, along the entire length of each section examined, at 12 dpi (Fig. 4J), and this was also observed for the extensive damage model at 30 dpi (Fig. 4J). As recovery time continued, the proportion of retinal sections showing laminar fusions declined, and did so significantly faster following selective damage than following extensive damage (Fig. 4J; $p<0.01$; two-sample Wilcoxon rank sum test). At the time of functional recovery (60–100 dpi), the selectively lesioned retinas displayed significantly fewer regions of laminar fusion than the extensively lesioned retinas (Fig. 4J).

Frequent rosette formation in regenerating retina after extensive but rarely after selective damage

The lamination analysis revealed several examples of highly disorganized retinal histology at post-functional recovery times following extensive, though not selective damage (Fig. 4). Because another goal of the present study is to evaluate long-term stability of the regenerated retina, we next evaluated regenerated retinas for the presence of retinal rosettes, which can be formed under various pathological and experimental conditions (Tulvatana et al., 1999). Retinal rosettes contain differentiated retinal cells which have become organized around a central lumen, but are not properly integrated into the retinal layers. To determine whether rosettes formed in either of our damage and regeneration models, we stained retinal cryosections with a combination of the cone photoreceptor marker zpr-1, and the nuclear stain DAPI. Twelve sections representing eyes collected at a range of sampling times from 100 to 300 dpi were inspected for the presence of rosettes, in which clusters of zpr-1 stained cells were positioned (abnormally) outside of the outer nuclear layer (see Methods). Rosettes were observed in sections processed from nearly all 16 fish subjected to extensive retinal damage (Fig. 4K–M; Table 2). However, only one example of a rosette was observed in sections processed from 22 fish subjected to selective retinal damage (Table 2). These results, together with those described for laminar fusions, are consistent with persistent retinal disorganization in retinas regenerating after extensive damage, as compared to progressive correction of lamination errors following lesions that do not destroy photoreceptors.

Overproduction of retinal neurons after extensive but not selective damage

In zebrafish retinas subjected to selective lesions, inner retinal neurons decrease in density following injury, and then increase as a function of recovery time (Fimbel et al., 2007). In retinas subjected to more extensive lesions, we observed a significantly higher density of Islet-1+ neurons in the GCL of retinal flat-mounts obtained at late recovery times. In order to directly compare the production of neurons in both lesion models, we stained retinal cryosections with an anti-HuC/D antibody, which labels postmitotic ganglion cells and amacrine cells (Marusich et al., 1994; Stenkamp et al., 2008a). Stained cells were counted in preparations obtained at 30, 60, 100, 160 and 210 dpi (n=6 fish at each sampling time), and densities of HuC/D+ neurons were calculated. Retinal regions having laminar fusions and rosettes were also used for this analysis. Neuronal densities were reduced at 30 dpi, in retinas regenerated after both extensive and selective damage, as compared to control retinas (Fig. 5), suggesting that, although inner retinal neurons were apparent at 12–14 dpi following these injuries (Fimbel et al., 2007; Sherpa et al., 2008), the full complement of these neurons was not yet restored even by 30 dpi. Following selective damage, at 60 dpi, the numbers of inner retinal neurons remained low in comparison to control, while extensively damaged retinas at 60 dpi the numbers of inner retinal neurons were restored to control levels. These data suggest that differences in the rate of production of neurons do not underlie the differences in the timing of functional recovery.

Interestingly, overproduction of inner retinal neurons was observed at late recovery times (160 and 210 dpi) following extensive damage. In contrast, there was no overproduction of inner retinal neurons following selective damage at late recovery times (Fig. 5), even in fish

sampled at 260 dpi (n=5; data not shown). Overproduction of neurons and the formation of rosettes at recovery times after the restoration of visual function, suggest defects in mechanisms responsible for controlling neuronal numbers and retinal organization during regeneration following an extensive lesion.

Temporal patterns of gene expression following extensive vs. selective retinal damage

Because several of the defects we observed in retinas regenerated following an extensive lesion were related to RGC production and axon growth and pathfinding, we wished to evaluate the expression of genes known to play roles in these processes during embryonic development. We and others have previously demonstrated that many genes related to RGC neurogenesis and differentiation, such as those encoding *ath5/atoh7*, *pax6*, islet-1, HuC/D protein, and neurolin/zn8, are expressed in regenerating retina in spatiotemporal patterns that recapitulate those seen in embryonic development (Fimbel et al., 2007; Sherpa et al., 2008). However, expression of some genes with known roles in embryonic RGC development, including *Brn3b*, *fgf8*, and *shha*, was not detected in regenerating retina in our previous study, using *in situ* hybridization (Sherpa et al., 2008). Therefore, in order to test whether any specific retinal gene may constitute a molecular correlate of the differences observed in the regeneration process following selective damage vs. extensive damage, we used the more sensitive method of real-time (quantitative) RT-PCR (qRT-PCR).

We measured expression of the genes *Brn3b*, *ath5*, *shha*, *fgf8a*, *ptc2a*, *Netrin*, and *KLF6a* by qRT-PCR using mRNA derived from extensively and selectively damaged eyes harvested at 1, 3, 6, 8, 12, and 20 dpi. *Brn3b* encodes a transcription factor expressed in a subset of RGCs (Erkman et al., 1996; Gan et al., 1996; Zhou et al., 1996) and it regulates RGC differentiation (DeCarvalho et al., 2004; Gan et al., 1996; Mu et al., 2004; Wang et al., 2002a). Following either extensive or selective retinal damage, this gene was significantly downregulated at 1, 3 and 6 dpi ($p<0.05$; Welch two sample t-test), and returned to levels statistically indistinguishable from controls at 8 dpi (Fig. 6A). This time-course likely reflects the loss of RGCs due to damage, and their reappearance due to regeneration (Fimbel et al., 2007; Sherpa et al., 2008), and further suggests that this gene does not likely underlie differences in functional recovery documented above.

Ath5/atoh7 encodes a bHLH transcription factor and is required for RGC neurogenesis in the zebrafish (Kay et al., 2001). After either extensive or selective retinal damage, this gene was significantly downregulated at 1 dpi. There was no significant difference in expression of *atoh7* at 3 dpi onward following selective damage as compared to control eyes. However, after extensive damage *atoh7* showed prolonged overexpression at later sampling times as compared to control eyes (Fig. 6B; $p<0.05$; Welch two sample t-test).

Sonic hedgehog (*shha*) mRNA is expressed by the RPE (Stenkamp et al., 2000), RGCs, and amacrine cells (Shkumatava et al., 2004) in embryonic zebrafish, is required for the progression of RGC differentiation (Neumann and Nuesslein-Volhard, 2000), regulation of RGC numbers (Zhang and Yang, 2001), directs the lamination of the retina (Wang et al., 2002b), and plays an indirect role in guiding embryonic RGC axons to the ONH (Stacher Horndli and Chien, 2012). Expression of *shha* was significantly downregulated following both extensive and selective damage at 3 and 6 dpi, and returned to control levels at 8 dpi

(Fig. 6C; $p < 0.05$). Interestingly, expression was again significantly downregulated following extensive damage at 12 dpi and 20 dpi as compared to expression in control eyes (Fig. 6C; $p < 0.05$).

Fgf8a is expressed in newly generated (embryonic) RGCs in zebrafish (Picker and Brand, 2005). Fgf signaling is involved in initiating a wave of RGC differentiation (McCabe et al., 1999) (Martinez-Morales et al., 2005), and is important for zebrafish photoreceptor survival and regeneration (Hochmann et al., 2012; Qin et al., 2011). After extensive retinal damage, the expression of *fgf8a* was significantly downregulated at 1, 3, 6 and 12 dpi, but after selective damage, this gene was downregulated only at 3 and 6 dpi (Fig. 6D) before returning to control levels.

The *ptc-2a* gene encodes a component of the cell-surface receptor complex for the hedgehog protein (Marigo et al., 1996), and is expressed by retinal neuroepithelial cells (Bibliowicz and Gross, 2009; Stenkamp et al., 2000). Following extensive damage, the expression of *ptc-2a* was significantly downregulated at 1 dpi, and following selective damage, the expression of this gene was significantly downregulated at 3 dpi (Fig. 6E), likely reflecting the loss of major sources of the Shh signal (RGCs and amacrine cells). However, the expression of this gene returned to control levels at the remaining recovery times following both types of damage (Fig. 6E).

Netrins are secreted axon guidance molecules; *netrin-1* is expressed by glial cells of the zebrafish ONH (Lauderdale et al., 1997; Strahle et al., 1997), and provides guidance for RGC axons, ensuring that they accurately enter into the ONH (Deiner et al., 1997). Following either extensive or selective retinal damage, the expression of *netrin-1* mRNA was significantly upregulated at 1 dpi (Fig. 6F; $p<0.05$). In the case of regeneration after selective damage, the expression of *netrin-1* returned to normal at 3 dpi, however following extensive damage *netrin-1* was significantly overexpressed at 12 and 20 dpi as compared to control eyes (Fig. 6F; $p < 0.05$).

KLF6a is a member of the Sp/KLF zinc finger transcription factor family (Bieker, 2001) and was identified as an important regulator of axon regeneration in adult zebrafish after optic nerve crush (Veldman et al., 2007). Following selective damage, this gene was significantly upregulated at 1 dpi (Fig. 6G). However, at all other recovery times, in both lesioning models, levels of expression of this gene remained statistically indistinguishable from those in control eyes.

To determine whether there were persistent abnormalities in gene expression following retinal regeneration, qRT-PCR was used to measure expression of the genes *brn3b*, *atoh7, shha, fgfa, ptc2a*, and *netrin-1*, using mRNA derived from extensively and selectively damaged eyes harvested at 100 dpi. At this time, numbers of HuC/D+ neurons have returned to control levels in both situations (Fig. 5). Levels of expression of all of these genes were remarkably consistent among control eyes vs. extensively damaged eyes vs. selectively damaged eyes (data not shown), with no significant differences detected (Welch two-sample t-tests).

In summary, these quantitative studies of gene expression during regeneration revealed *atoh7*, *shha*, *fgf8a*, and *netrin-1* as potential molecular mediators of retinal regeneration over the time frame prior to functional recovery. Delayed functional recovery and persistent histological abnormalities following an extensive lesion are therefore correlated with overexpression of *atoh7* and *netrin-1*, and with reduced expression of *shha* and *fgf8a*.

Distribution of Hedgehog (Hh) protein following extensive vs. selective retinal damage

To further assess potential roles of Shh signaling in the regulation of the regeneration process, we wished to determine the distribution of Hh protein in adult undamaged and regenerating zebrafish retinas. We used indirect immunofluorescence with an anti-zebrafish Shh polyclonal antibody (see Methods). This antibody identifies processed (N-terminal) and unprocessed Shh in HEK293S cells transfected with zebrafish Shh, as indicated by Western blotting results provided in the manufacturer's data sheet. We verified that this antibody identifies Shh within zebrafish tissues by Western blotting with zebrafish embryo protein extracts. The anti-zebrafish Shh antibody detected bands of approximately 50 kDa and 20 kDa (Fig. 7A); these molecular sizes correspond with known sizes of unprocessed and processed Shh of chick and mouse (Marti et al., 1995). Therefore, the anti-zebrafish Shh antibody likely detects both processed and unprocessed Shh in zebrafish tissues. Because this antibody may cross-react with Shhb (also known as Tiggy-winkle hedgehog) and Indian hedgehog (Ihh), the following experiments provided information regarding the distribution of all Hh protein. In embryonic zebrafish, this antibody stains midline structures (data not shown), and stains the NFL, the plexiform layers, outer limiting membrane, the circumferential germinal zone (CGZ), and the RPE in the larval zebrafish eye (Fig. 7B–C). The distribution in the NFL, plexiform layers, and RPE is consistent with known patterns of expression of *shha* and *shhb/twhh* mRNA, and/or those of *shha* reporter constructs – in the RPE (Stenkamp et al., 2000), the GCL (Neumann and Nuesslein-Volhard, 2000), and amacrine cells (Shkumatava et al., 2004). However, the staining pattern reported here suggests targeting and/or accumulation of Hh proteins in synaptic layers and the NFL. Hh staining within the CGZ is consistent with the known pattern of expression of *ptc-2* mRNA (Bibliowicz and Gross, 2009; Stenkamp et al., 2000), which encodes a component of the Hh receptor complex (Concordet et al., 1996).

Undamaged adult retinas displayed a diffuse pattern of Hh labeling associated with all plexiform layers, the outer limiting membrane, and the interphotoreceptor matrix, along with punctate staining of the RPE, and weak fluorescence of photoreceptor inner segments (Fig. 7D–E). In addition, more intense labeling was found in the NFL, where myelinated RGC axons are located (Munzel et al., 2012) (Fig. 7D–E). Control experiments performed in the absence of detergent confirmed that the anti-Shh antibody recognized extracellular Hh in adult retina, predominantly in the NFL (Fig. 7F), and experiments without primary antibody indicated that this staining pattern is specific, with the exception of autofluorescence of photoreceptor inner segments (Fig. 7G). To our knowledge, this is the first report of the spatial pattern of expression of any Hh protein or mRNA in adult vertebrate retina, *in vivo*. The distribution of Hh immunofluorescence within the NFL is consistent with the targeting of Hh protein to the surface of axons of RGCs, as determined in cultures of mouse retinal neurons (Beug et al., 2011).

Retinas undergoing regeneration following selective damage, sampled at 14 and 30 dpi, showed a pattern of Hh distribution similar to that seen in undamaged retina (Fig. 7H–K), with the staining of greatest intensity in the NFL and more diffuse staining in the regenerating plexiform layers. Retinas regenerating as a consequence of extensive damage showed weaker staining of the regenerating plexiform layers, and lacked prominent staining at the vitreal surface, where the NFL resides (Fig. 7L–O). Because our examination of *gap43*:GFP+ axons in whole mounted regenerating retinas suggested that a nerve fiber layer may be only sporadically encountered in sectioned retinas subjected to an extensive lesion (Fig. 3), we very thoroughly sampled these retinas for Hh immunoreactivity and were able to locate rare regions of Hh staining on the vitreal surface that were likely associated with RGC axons (Fig. 7P–S). These results are consistent with the quantitative findings regarding *shha* mRNA expression (Fig. 6C), and reveal that potentially key sites of Hh protein abundance are not rapidly re-established in retinas regenerating following extensive damage as compared to selective damage. It is possible that the RGCs initially generated do not synthesize Hh protein, and/or do not properly target its secretion. Extensively damaged retinas processed at 30 dpi also showed ectopic patches of Hh staining that were associated with histological abnormalities (Fig. 7N–O), suggesting that the spatial distribution of Hh becomes progressively more irregular during the regeneration process.

Reduced Shh signaling delays functional regeneration after selective damage

To test the hypothesis that retinal Shh signaling is necessary for rapid functional retinal regeneration, we used an adult clutch of heterozygous *shha*^{t4}+/− zebrafish (n=4) and their *shha*+/+ siblings (n=6). The retinas of *shha*^{t4}+/− zebrafish express reduced levels of both *shha* and *ptc-2a* mRNA (Stenkamp et al., 2008b), indicating reduced Shh signaling (Concordet et al., 1996). To maximize statistical power using this small number of identified heterozygous fish and their homozygous wild-type siblings, we used unilateral selective lesion and monitored the DLR (instead of bilateral selective lesion and the place-preference assay) over a 105 day recovery period. Recovery of the DLR in general took place asynchronously in this experiment. Within the clutch of otherwise genotypically matched fish, recovery of the DLR required significantly longer time in the heterozygous *shha*^{t4}+/− fish as compared with their *shha*+/+ siblings (Fig. 8A; p=0.001; logistic regression with repeated measures).

In separate experiments we verified that *shha*^{t4}+/− retinas experience retinal damage that spares photoreceptors, Müller glia, and small numbers of horizontal cells, similar to that of wild-type retinas, following selective lesioning with ouabain (Fig. 8B). We also established that *shha*^{t4}+/− retinas show evidence of histological regeneration, albeit with laminar fusions, at 14 days after the injury, also similar to the situation in wild-type retinas [Fig. 8C, compare to (Fimbel et al., 2007)]. We then evaluated the distribution of Hh protein in five regenerating *shha*^{t4}+/− retinas following selective damage to the inner retinal layers. At 14 dpi, the regenerating, selectively damaged *shha*^{t4}+/− retinas displayed a distribution of Hh immunoreactivity similar to that of extensively damaged wild-type retinas (Fig. 8C, compare to Fig. 7), with more diffuse and weaker staining of the regenerating plexiform layers, NFL, and RPE. These data suggest that reduced Hh signaling in specific retinal layers may be

related to the delay in functional regeneration of the *shha*^{t4}+/− retina following a neurotoxic lesion that destroys the inner retina but permits survival of photoreceptors.

No hypertrophy of optic nerve head after selective damage

Our previous study showed that the diameter of the ONH continues to enlarge to abnormal proportions at later recovery times following extensive damage (Sherpa et al., 2008). In order to test whether the ONH experiences hypertrophy at later recovery times following selective retinal damage that spares photoreceptors, we measured ONH diameters in regenerating retinas at 8, 30, 60, 100, 160, 195, and 222 days after selective lesioning (n=6 fish at each sampling time). Our results for early recovery times are consistent with those of Fimbel et al. (Fimbel et al., 2007) (Supplemental Fig. 3), as the ONH did not disappear – as with the extensive retinal lesion (Sherpa et al., 2008) – but instead shrank slightly before returning to normal dimensions. At later recovery times, diameters of ONHs of selectively damaged retinas were not significantly larger than those of undamaged, control eyes (Supplemental Fig. 3C,D,E; one-sided Dunnett test). These results indicate that ONH hypertrophy does not take place following a lesion that is selective for inner retinal layers.

Misrouted axons and ectopic neurons in optic nerve head after extensive damage

We next turned our attention to the composition of the ONHs observed at post-functional recovery sampling times following extensive retinal damage (Sherpa et al., 2008). To address whether RGCs continue to project axons to the ONH, and whether these axons successfully traverse the ONH, we processed retinal sections with the zn8 antibody, which stains the cell adhesion molecule neurolin/DM-grasp, found on growing axons (Mann et al., 2006). Zn8 staining was only rarely and weakly found in control ONHs, (Fig. 9A; n=4), and in ONHs of selectively damaged retinas processed at 222 dpi (Fig. 9E; n=5), but was observed in all ONHs of extensively lesioned retinas processed at 222 dpi (n=3) and 263 dpi (n=3). Interestingly, zn8 staining revealed tangles of axons that appeared to terminate within the ONH (Fig. 9I). Axon tangles were also observed in ONHs processed at times (133 dpi) closer to the time of functional recovery (data not shown).

To determine whether astrocytes were present at the ONH, we processed sections with the zrf-1 antibody, which labels both astrocytes and Müller glia (Marcus and Easter, 1995). Control ONHs and ONHs in retinas regenerated after selective damage all showed astrocyte processes spanning the ONH at approximately right angles to the optic nerve (Fig. 9B,F). However, ONHs in retinas regenerated after an extensive lesion displayed fewer astrocyte processes, which did not completely span the ONH (Fig. 9J).

DAPI staining of the ONHs of extensively damaged retinas frequently revealed large numbers of nuclei as compared with those of controls or selectively damaged retinas (compare Figs. 9I,J to Figs. 9A,B,E,F), prompting us to assess whether neurons had invaded the ONH, using the HuC/D neuronal marker. Control ONHs did not contain HuC/D+ neurons (Fig. 9C), and the ONHs of selectively damaged retinas contained a small number of HuC/D+ neurons (Fig. 9G). In contrast, the enlarged ONHs of extensively damaged retinas contained clusters of HuC/D+ neurons (Fig. 9K). Smaller clusters of ectopic neurons

were observed in ONHs processed at times (133 dpi) closer to the time of functional recovery (data not shown).

Finally, we performed Hh staining experiments on ONHs of retinas processed at well after the recovery of visual function. Control ONHs displayed moderate staining of the NFL in the region approaching the ONH, and this staining increased in intensity within the ONH (Fig. 9D). A similar pattern was observed in ONHs of selectively damaged retinas processed at 222 dpi (Fig. 9H). The ONHs of extensively damaged retinas did show staining of the approaching NFL, and strong staining within the ONH, but much of this staining was associated with fibers that did not successfully navigate through the ONH (Fig. 9L).

In summary, retinal regeneration following an extensive lesion that spares only Müller glia ultimately results in histological abnormalities within an enlarged ONH. These abnormalities include ectopic neurons, misrouted axons, and astrocytes that do not span the ONH.

Discussion

Retinal regeneration is facilitated by the presence of surviving retinal neurons

The findings of the present study support the hypothesis that more favorable functional and long-term histological outcomes of regeneration are realized following a more limited extent of damage. The initial damage caused by 2 μM ouabain spares Müller glia, photoreceptors, and the occasional horizontal cell whereas the damage caused by 10 μM ouabain results in widespread destruction of all retinal neurons, and the sparing of only Müller glia (Fig. 1). In both types of damage, a 1–4 day period of cell death induces the surviving Müller glia to re-enter the cell cycle (Fimbel et al., 2007) (Fig. 1; Supplemental Fig. 1), and initiate a 3–12 day period of robust proliferation (Fimbel et al., 2007; Sherpa et al., 2008). Following both types of damage, restoration of some retinal lamination is evident by 12–14 dpi (Fimbel et al., 2007; Sherpa et al., 2008). However, the different types of damage also result in several distinct outcomes (summarized in Table 3).

The most striking and perhaps most important difference in outcome is the more rapid recovery of visual function following selective retinal damage – nearly twice the recovery rate. This remarkable difference is not directly related to the initial need to produce fewer neurons following selective damage, because in both lesioning paradigms, recovery of retinal lamination (albeit with errors) was achieved at 12–14 days after damage (Fimbel et al., 2007; Sherpa et al., 2008) (see also Fig. 7H,L,P). In the present study we tested potential alternative mechanisms that may underlie the delay in functional recovery following extensive damage. One potential mechanism that is discounted by our data, is a slower rate of neuronal production in extensively damaged retinas. Rather, our results suggest that Müller glia re-enter the cell cycle after extensive damage (Fig. 1G; Supplemental Fig. 1), and that the restoration of HuC/D+ neuronal density was actually achieved more rapidly after extensive damage than after selective damage (Fig. 5). Therefore, slower production of neurons does not underlie delayed functional recovery.

A second mechanism, one which is supported by our data, is the impairment of functional recovery by persistent histological disorganization. Errors in histology of regenerated retina have been previously reported. Widespread damage of the goldfish retina with ouabain results in regenerated retinas having some cells misplaced within the inner plexiform layer (Raymond et al., 1988), and errors in two-dimensional photoreceptor pattern are also quite severe (Stenkamp and Cameron, 2002; Stenkamp et al., 2001). Retinas that regenerate following surgical lesions also contain laminar fusions (goldfish) (Hitchcock et al., 1992), and abnormal photoreceptor patterns (zebrafish) (Stenkamp and Cameron, 2002). The current study is the first to evaluate histological errors as a function of lesion type and of recovery time. Although lamination is highly disrupted following both treatments at early recovery times, selectively damaged retinas ultimately recover normal lamination almost entirely (and this recovery is significant at the time of restoration of visual function), while large regions of extensively damaged retinas fail to recover proper lamination. One possible mechanism for this corrective process is that of selective cell death as synaptogenesis proceeds and cells with abnormal positions or connections are eliminated. Although the embryonic zebrafish retina displays a very limited amount of cell death (Biehlmaier et al., 2001), other vertebrate retinas experience widespread waves of cell death to remove neurons with inappropriate or no connections (Farah, 2006). An alternative mechanism is that of late cellular migration to the appropriate layer, again a phenomenon not documented in the embryonic zebrafish retina, but there is support for this mechanism in other vertebrate taxa (Reese and Galli-Resta, 2002). In either case, this progressive correction of lamination errors following selective damage suggests that some of the cellular mechanisms involved in the regeneration of a functional retina may be distinct from those involved in embryonic retinal development.

Strongly supported by our data is a third potential mechanism underlying the delay in functional recovery after extensive damage: defects in axon growth and pathfinding toward and then within the ONH. In extensively damaged retinas, *gap43:GFP*+ axon bundles displayed delayed and sporadic pathfinding to the ONH at 21 dpi, and showed trajectories with greater complexity at 53 dpi, than their selectively damaged counterparts (Fig. 3). Similarly, wayward “looping” patterns were also observed in regenerated RGC axons following a chemical lesion in goldfish retina (Stuermer, 1988). In addition, the ONHs of retinas that regenerated following an extensive lesion displayed tangled neural processes (Fig. 9), suggesting that some RGC axons may not successfully traverse the ONH. We speculate that delayed axon growth and axon misrouting within the retina and ONH may therefore result in delays in RGC axons reaching the targets in the brain that mediate the visual behaviors we assayed. Therefore, although new retinal neurons are produced rapidly and in abundance after extensive damage, and express the RGC-related mRNAs/proteins *atoh/ath5*, *Brn3b*, HuC/D, *Klf6a*, and islet1 (Fig. 6; Sherpa et al., 2008), they fail to generate axons that efficiently navigate to and through the ONH. Potential roles for RGC-related genes that were differentially expressed in extensively vs. selectively damaged retina will be discussed in the next section.

An additional set of distinctive regenerative outcomes of regeneration following extensive vs. selective damage concerns the long-term histological stability of the retina and ONH. At

late recovery times, extensively lesioned retinas overproduced neurons (Fig. 5), retained laminar fusions, developed rosettes (Fig. 4 and Table 2), and displayed ONHs with ectopic neurons and misrouted axons (Fig. 9). Selective damage resulted in none of these apparently hyperplastic outcomes (Table 3). Retinal rosettes have been documented in rainbow trout during regeneration after intraocular injection of ouabain (Kurz-Isler and Wolburg, 1982), and are a classic histological finding in retinoblastoma, retinal dysplasia (Chan et al., 2007), and retinal detachment in humans (Tulvatana et al., 1999). Despite resulting from a number of different human diseases, the mechanisms of rosette formation are still unknown, although defects in Shh signaling have been implicated (Chan et al., 2007) and will be further discussed in the next section.

We previously proposed that ONH hypertrophy may be a consequence of lack of control of RGC production (Sherpa et al., 2008) and that the resultant supernumerary axons enlarged the ONH. However, the present study suggests that instead the enlarged ONHs contain tangled axons and ectopic neurons, which likely account for much of the additional ONH size.

The present study, therefore, provides evidence that events required for functional recovery and long-term histological stability are facilitated in selectively damaged retinas, as compared to extensively damaged retinas. These outcomes suggest that neurons that survive the lesion in selectively damaged retinas may provide structural or molecular cues to the regenerating cells regarding neuronal differentiation, retinal patterning and the regulation of neuronal numbers, axon pathfinding and the establishment of accurate synaptic connections.

An alternative, or additional possibility is that more rapid functional recovery is facilitated by the persistent presence of a remnant ONH following selective lesion (Fimbel et al., 2007; Sherpa et al., 2008).The time to functional recovery is tightly correlated with the time to restoration of the original size of the ONH: at 60 days following selective damage and at 100 days following extensive damage (Table 3). In order to restore the ONH in each case, RGC axons must navigate from newly-generated ganglion cell bodies, through an environment that has likely been affected by the lesioning process, and over a considerable distance. This navigational process is clearly impaired in extensively damaged retinas, but not in selectively damaged retinas (Fig. 3; 9). It is possible that structural or molecular information derived from the presence of a remnant ONH that survived the selective lesion may promote the proper expression of - or act as the source of - these factors that guide axons of regenerated RGCs. In the case of extensive damage, some of these control mechanisms may malfunction and this may explain the delay in axon growth, delayed restoration of ONH size, and delayed functional recovery. However, the presence of a remnant ONH does not likely explain the long-term histological stability of the retina in selectively damaged retinas.

The behavioral and histological findings reported here have implications for the field of regenerative medicine, as vision science progresses toward treatments of human visual disorders that utilize cell replacement or regenerative therapies (Ahmad et al., 2011; Karl et al., 2008; Song et al., 2013). These therapies must produce regenerated retinal neurons that achieve appropriate and functional synaptic connections, and do not result in hyperplastic

outcomes. Regenerative therapies for glaucoma represent additional challenges due to the need to replace dead or damaged RGCs, cells which must generate long axons and reach targets outside of the eye (Al-Shamekh and Goldberg, 2013). While the lesioning paradigms used in the present study do not directly model glaucoma, our results suggest the most optimal strategies for regenerative interventions must be applied prior to extensive retinal damage, to take advantage of patterning information provided by any surviving retinal neurons.

Sonic hedgehog signaling facilitates retinal regeneration

The expression levels of several genes involved in RGC development were differentially regulated over a 20 day period following extensive vs. selective damage. In extensively damaged retinas, *atoh7/ath5* and *netrin-1* were upregulated, while *shha* and *fgf8a* were downregulated (Fig. 6), and thus constitute molecular correlates of delayed functional regeneration. We speculate that prolonged upregulation of *atoh7* may contribute to the overproduction of inner retinal neurons, as this gene is known to promote RGC fates (Sapkota et al., 2011; Song et al., 2013). Upregulation of *netrin-1* may disrupt RGC axon passage through the ONH, where *netrin-1* is normally expressed (Mann et al., 2004). Reduced expression of *shha* may also contribute to the overproduction of retinal neurons; this gene is an important regulator of retinal neurogenesis and neuronal number (Zhang and Yang, 2001). In addition, in retinas regenerating following an extensive lesion, the normal distribution and apparent levels of Hh protein, particularly in the regenerating NFL, were not restored (Fig. 7). Together with the delay in functional recovery in $shha^{t4}$+/– zebrafish subjected to a selective lesion (Fig. 8), these data support roles for Shh signaling in promoting rapid recovery of visual function and histological accuracy in the regenerating zebrafish retina.

Vertebrate *shh* genes have multiple roles in retinal development including the regulation of RGC number (Neumann and Nuesslein-Volhard, 2000; Zhang and Yang, 2001), promotion of accurate retinal patterning (Stenkamp et al., 2008a; Wang et al., 2002b), concentration-dependent effects on growth of RGC axons (Charron et al., 2003), astrocyte development in the ONH (Wallace and Raff, 1999), and guidance of RGC axons, indirectly mediated by factors at the ONH that are regulated by Shh (Stacher Horndli and Chien, 2012). During retinal regeneration in the embryonic chick, inhibition of Shh signaling resulted in an increase in the number of regenerated RGCs (Spence et al., 2004), consistent with the results reported here. It is remarkable that errors in regulation of neuronal number, retinal organization, and restoration and maintenance of ONH size and composition are all observed following extensive but not selective damage. Together these findings implicate Shh signaling as an important molecular correlate of optimized retinal regeneration. For example, reduced Shh signaling may result in the dysregulation of neuronal production, leading to the generation of supernumerary neurons following extensive retinal damage. Reduced Shh signaling may also contribute to the formation and persistence of histological defects, such as those seen in mouse retina that develops following RGC-specific ablation of *shh* expression (Wang et al., 2002b), and in a human retinal dysplasia associated with Patau Syndrome/trisomy13 (Chan et al., 2007). Finally, reduced RGC-derived Shh may delay RGC axon growth, the restoration of the ONH, and the recovery of visual function following

extensive retinal damage. It is surprising that the *ptc-2a* gene was not coordinately under-expressed in the broad damage model (Fig. 6); this outcome may be related to the use of a highly heterogeneous tissue (whole eyes) in the qRT-PCR analysis.

The distribution of Hh immunoreactivity in adult zebrafish retina is reported here for the first time. In undamaged retina this distribution included extracellular aspects of the NFL, the plexiform layers, and the RPE (Fig. 7). These results are consistent with the known distribution of *shha* and *twhh* mRNA in embryonic zebrafish in RGCs, amacrine cells, and the RPE (Shkumatava et al., 2004; Stenkamp et al., 2000) and further suggest targeting or accumulation of Hh protein in synaptic layers.

Adequate Hh signaling during retinal regeneration is required for rapid functional recovery, as heterozygous carriers of a *shha* deletion mutation (*shha*^{t4}+/−), in which Hh signaling is chronically reduced (Stenkamp et al., 2008a), show a significant delay in recovery of visual function following selective damage, as compared with their wild-type siblings (Fig. 8). The requirement for sufficient Hh may be related to signaling associated with the developing RGC layer, because reduced Hh staining was observed in the inner plexiform and NFL layers in regenerating *shh*^{t4}+/− retinas (Fig. 7). However, this specific genotype (*shh*^{t4}+/−, a.k.a. *syu*^{t4}+/−) also shows a progressive and age-related cone loss phenotype, which becomes evident in zebrafish two years of age and older (Stenkamp et al., 2008a). Although the fish used in the injury experiments of the present study were younger than the age of onset of the cone loss condition, it remains possible that delays in functional recovery following injury to *shha*^{t4}+/− retinas may be related to this progressive cone pathology, and/or to reduced Hh signaling in the RPE/outer retina. It is interesting that the heterozygous condition at the *shha* locus supports normal retinal development and function, yet contributes to cone loss in aging fish, and delayed recovery of visual function following retinal injury.

Supplementary Material

Refer to Web version on PubMed Central for supplementary material.

Acknowledgments

The authors thank Ms. Andrea Ansari, Mr. Shawn Robison, and Mr. Matthew Singer (U. Idaho) for technical assistance, Drs. David Hyde (U. Notre Dame) and Peter Fuerst (U. Idaho) for critically evaluating earlier versions of this manuscript, and Dr. Christopher Williams (U. Idaho) for assistance with statistics. This work was supported by NIH R01 EY012146 (DLS), The Glaucoma Foundation (DLS), a Multicultural Fellowship from the University of Idaho (TS), a graduate fellowship from Idaho's NIHINBRE program, P20 RR016454 (SSH), and an award to TL from the U. Idaho's student grant program. Ms. Ansari was supported by an NSF REU in Computational Neuroscience & Technology, NSF 0243885, and Mr. S. Robison was supported by an undergraduate internship from Idaho's NIH-INBRE program. The Zebrafish International Resource Center (ZIRC) was the source of the *shha*^{t4} line, the *GFAP:GFP* line, and the antibodies zpr-1, zn8, and zrf-1, and is supported by NIH P40 RR012546.

REFERENCES

Ahmad I, Del Debbio CB, Das AV, Parameswaran S. Muller glia: a promising target for therapeutic regeneration. Investigative ophthalmology & visual science. 2011; 52:5758–5764. [PubMed: 21803967]

Al-Shamekh S, Goldberg JL. Retinal repair with induced pluripotent stem cells. Translational research : the journal of laboratory and clinical medicine. 2013

Bailey TJ, Fossum SL, Fimbel SM, Montgomery JE, Hyde DR. The inhibitor of phagocytosis, O-phospho-L-serine, suppresses Muller glia proliferation and cone cell regeneration in the light-damaged zebrafish retina. Experimental eye research. 2011; 91:601–612. [PubMed: 20696157]

Benner MJ, Drew RE, Hardy RW, Robison BD. Zebrafish (Danio rerio) vary by strain and sex in their behavioral and transcriptional responses to selenium supplementation. Comp Biochem Physiol A Mol Integr Physiol. 2010; 157:310–318. [PubMed: 20659579]

Bernardos RL, Barthel LK, Meyers JR, Raymond PA. Late-stage neuronal progenitors in the retina are radial Muller glia that function as retinal stem cells. J Neurosci. 2007; 27:7028–7040. [PubMed: 17596452]

Bernardos RL, Raymond PA. GFAP transgenic zebrafish. Gene Expr Patterns. 2006; 6:1007–1013. [PubMed: 16765104]

Beug ST, Parks RJ, McBride HM, Wallace VA. Processing-dependent trafficking of Sonic hedgehog to the regulated secretory pathway in neurons. Molecular and cellular neurosciences. 2011; 46:583–596. [PubMed: 21182949]

Bibliowicz J, Gross JM. Expanded progenitor populations, vitreo-retinal abnormalities, and Muller glial reactivity in the zebrafish leprechaun/patched2 retina. BMC developmental biology. 2009; 9:52. [PubMed: 19840373]

Biehlmaier O, Neuhauss SC, Kohler K. Onset and time course of apoptosis in the developing zebrafish retina. Cell and tissue research. 2001; 306:199–207. [PubMed: 11702231]

Bieker JJ. Kruppel-like factors: three fingers in many pies. The Journal of biological chemistry. 2001; 276:34355–34358. [PubMed: 11443140]

Braisted JE, Essman TF, Raymond PA. Selective regeneration of photoreceptors in goldfish retina. Development. 1994; 120:2409–2419. [PubMed: 7956821]

Cameron DA, Carney LH. Cell mosaic patterns in the native and regenerated inner retina of zebrafish: implications for retinal assembly. The Journal of comparative neurology. 2000; 416:356–367. [PubMed: 10602094]

Cameron DA, Easter SS Jr. Cone photoreceptor regeneration in adult fish retina: phenotypic determination and mosaic pattern formation. J Neurosci. 1995; 15:2255–2271. [PubMed: 7891164]

Chan A, Lakshminrusimha S, Heffner R, Gonzalez-Fernandez F. Histogenesis of retinal dysplasia in trisomy 13. Diagnostic pathology. 2007; 2:48. [PubMed: 18088410]

Charron F, Stein E, Jeong J, McMahon AP, Tessier-Lavigne M. The morphogen sonic hedgehog is an axonal chemoattractant that collaborates with netrin-1 in midline axon guidance. Cell. 2003; 113:11–23. [PubMed: 12679031]

Concordet JP, Lewis KE, Moore JW, Goodrich LV, Johnson RL, Scott MP, Ingham PW. Spatial regulation of a zebrafish patched homologue reflects the roles of sonic hedgehog and protein kinase A in neural tube and somite patterning. Development (Cambridge, England). 1996; 122:2835–2846.

DeCarvalho AC, Cappendijk SL, Fadool JM. Developmental expression of the POU domain transcription factor Brn-3b (Pou4f2) in the lateral line and visual system of zebrafish. Dev Dyn. 2004; 229:869–876. [PubMed: 15042710]

Deiner MS, Kennedy TE, Fazeli A, Serafini T, Tessier-Lavigne M, Sretavan DW. Netrin-1 and DCC mediate axon guidance locally at the optic disc: loss of function leads to optic nerve hypoplasia. Neuron. 1997; 19:575–589. [PubMed: 9331350]

Erkman L, McEvilly RJ, Luo L, Ryan AK, Hooshmand F, O'Connell SM, Keithley EM, Rapaport DH, Ryan AF, Rosenfeld MG. Role of transcription factors Brn-3.1 and Brn-3.2 in auditory and visual system development. Nature. 1996; 381:603–606. [PubMed: 8637595]

Farah MH. Neurogenesis and cell death in the ganglion cell layer of vertebrate retina. Brain research reviews. 2006; 52:264–274. [PubMed: 16764935]

Fausett BV, Goldman D. A role for alpha1 tubulin-expressing Muller glia in regeneration of the injured zebrafish retina. J Neurosci. 2006; 26:6303–6313. [PubMed: 16763038]

Fimbel SM, Montgomery JE, Burket CT, Hyde DR. Regeneration of inner retinal neurons after intravitreal injection of ouabain in zebrafish. J Neurosci. 2007; 27:1712–1724. [PubMed: 17301179]

Fischer AJ, Bongini R. Turning Muller glia into neural progenitors in the retina. Molecular neurobiology. 2011; 42:199–209. [PubMed: 21088932]

Gan L, Xiang M, Zhou L, Wagner DS, Klein WH, Nathans J. POU domain factor Brn-3b is required for the development of a large set of retinal ganglion cells. Proc Natl Acad Sci U S A. 1996; 93:3920–3925. [PubMed: 8632990]

Hitchcock PF, Lindsey Myhr KJ, Easter SS Jr. Mangione-Smith R, Jones DD. Local regeneration in the retina of the goldfish. Journal of neurobiology. 1992; 23:187–203. [PubMed: 1527527]

Hochmann S, Kaslin J, Hans S, Weber A, Machate A, Geffarth M, Funk RH, Brand M. Fgf signaling is required for photoreceptor maintenance in the adult zebrafish retina. PloS one. 2012; 7:e30365. [PubMed: 22291943]

Hothorn T, Bretz F, Westfall P. Simultaneous inference in general parametric models. Biometrical journal. Biometrische Zeitschrift. 2008; 50:346–363. [PubMed: 18481363]

Jones BW, Kondo M, Terasaki H, Lin Y, McCall M, Marc RE. Retinal remodeling. Japanese journal of ophthalmology. 2012

Karl MO, Hayes S, Nelson BR, Tan K, Buckingham B, Reh TA. Stimulation of neural regeneration in the mouse retina. Proceedings of the National Academy of Sciences of the United States of America. 2008; 105:19508–19513. [PubMed: 19033471]

Kassen SC, Ramanan V, Montgomery JE, T.B. C, Liu CG, Vihtelic TS, Hyde DR. Time course analysis of gene expression during light-induced photoreceptor cell death and regeneration in albino zebrafish. Developmental neurobiology. 2007; 67:1009–1031. [PubMed: 17565703]

Kay JN, Finger-Baier KC, Roeser T, Staub W, Baier H. Retinal ganglion cell genesis requires lakritz, a Zebrafish atonal Homolog. Neuron. 2001; 30:725–736. [PubMed: 11430806]

Kurz-Isler G, Wolburg H. Morphological study on the regeneration of the retina in the rainbow trout after ouabain-induced damage: evidence for dedifferentiation of photoreceptors. Cell and tissue research. 1982; 225:165–178. [PubMed: 7116425]

Kutzing MK, Langhammer CG, Luo V, Lakdawala H, Firestein BL. Automated Sholl analysis of digitized neuronal morphology at multiple scales. Journal of visualized experiments : JoVE. 2010

Lauderdale JD, Davis NM, Kuwada JY. Axon tracts correlate with netrin-1a expression in the zebrafish embryo. Mol Cell Neurosci. 1997; 9:293–313. [PubMed: 9268507]

Lenkowski JR, Qin Z, Sifuentes CJ, Thummel R, Soto CM, Moens CB, Raymond PA. Retinal regeneration in adult zebrafish requires regulation of TGFbeta signaling. Glia. 2013; 61:1687–1697. [PubMed: 23918319]

Lindsey AE, Powers MK. Visual behavior of adult goldfish with regenerating retina. Visual neuroscience. 2007; 24:247–255. [PubMed: 17592671]

Longair MH, Baker DA, Armstrong JD. Simple Neurite Tracer: open source software for reconstruction, visualization and analysis of neuronal processes. Bioinformatics. 2011; 27:2453–2454. [PubMed: 21727141]

Maier W, Wolburg H. Regeneration of the goldfish retina after exposure to different doses of ouabain. Cell and tissue research. 1979; 202:99–118. [PubMed: 509506]

Mann CJ, Hinits Y, Hughes SM. Comparison of neurolin (ALCAM) and neurolin-like cell adhesion molecule (NLCAM) expression in zebrafish. Gene Expr Patterns. 2006; 6:952–963. [PubMed: 16750657]

Mann F, Harris WA, Holt CE. New views on retinal axon development: a navigation guide. The International journal of developmental biology. 2004; 48:957–964. [PubMed: 15558486]

Marcus RC, Delaney CL, Easter SS Jr. Neurogenesis in the visual system of embryonic and adult zebrafish (Danio rerio). off. Visual neuroscience. 1999; 16:417–424. [PubMed: 10349963]

Marcus RC, Easter SS Jr. Expression of glial fibrillary acidic protein and its relation to tract formation in embryonic zebrafish (Danio rerio). The Journal of comparative neurology. 1995; 359:365–381. [PubMed: 7499535]

Marigo V, Davey RA, Zuo Y, Cunningham JM, Tabin CJ. Biochemical evidence that patched is the Hedgehog receptor. Nature. 1996; 384:176–179. [PubMed: 8906794]

Marti E, Takada R, Bumcrot DA, Sasaki H, McMahon AP. Distribution of Sonic hedgehog peptides in the developing chick and mouse embryo. Development (Cambridge, England). 1995; 121:2537–2547.

Martinez-Morales JR, Del Bene F, Nica G, Hammerschmidt M, Bovolenta P, Wittbrodt J. Differentiation of the vertebrate retina is coordinated by an FGF signaling center. Dev Cell. 2005; 8:565–574. [PubMed: 15809038]

Marusich MF, Furneaux HM, Henion PD, Weston JA. Hu neuronal proteins are expressed in proliferating neurogenic cells. J Neurobiol. 1994; 25:143–155. [PubMed: 7517436]

McCabe KL, Gunther EC, Reh TA. The development of the pattern of retinal ganglion cells in the chick retina: mechanisms that control differentiation. Development. 1999; 126:5713–5724. [PubMed: 10572047]

Mensinger AF, Powers MK. Visual function in regenerating teleost retina following cytotoxic lesioning. Visual neuroscience. 1999; 16:241–251. [PubMed: 10367959]

Meyers JR, Hu L, Moses A, Kaboli K, Papandrea A, Raymond PA. beta-catenin/Wnt signaling controls progenitor fate in the developing and regenerating zebrafish retina. Neural development. 2012; 7:30. [PubMed: 22920725]

Montgomery JE, Parsons MJ, Hyde DR. A novel model of retinal ablation demonstrates that the extent of rod cell death regulates the origin of the regenerated zebrafish rod photoreceptors. The Journal of comparative neurology. 2011; 518:800–814. [PubMed: 20058308]

Mu X, Beremand PD, Zhao S, Pershad R, Sun H, Scarpa A, Liang S, Thomas TL, Klein WH. Discrete gene sets depend on POU domain transcription factor Brn3b/Brn-3.2/POU4f2 for their expression in the mouse embryonic retina. Development. 2004; 131:1197–1210. [PubMed: 14973295]

Munzel EJ, Schaefer K, Obirei B, Kremmer E, Burton EA, Kuscha V, Becker CG, Brosamle C, Williams A, Becker T. Claudin k is specifically expressed in cells that form myelin during development of the nervous system and regeneration of the optic nerve in adult zebrafish. Glia. 2012; 60:253–270. [PubMed: 22020875]

Nagashima M, Barthel LK, Raymond PA. A self-renewing division of zebrafish Muller glial cells generates neuronal progenitors that require N-cadherin to regenerate retinal neurons. Development (Cambridge, England). 2013; 140:4510–4521.

Negishi K, Teranishi T, Kato S, Nakamura Y. Immunohistochemical and autoradiographic studies on retinal regeneration in teleost fish. Neurosci Res Suppl. 1988; 8:S43–57. [PubMed: 3231367]

Nelson CM, Ackerman KM, O'Hayer P, Bailey TJ, Gorsuch RA, Hyde DR. Tumor necrosis factor-alpha is produced by dying retinal neurons and is required for Muller glia proliferation during zebrafish retinal regeneration. J Neurosci. 2013; 33:6524–6539. [PubMed: 23575850]

Neumann CJ, Nuesslein-Volhard C. Patterning of the zebrafish retina by a wave of sonic hedgehog activity. Science (New York, N.Y. 2000; 289:2137–2139.

Ooto S, Akagi T, Kageyama R, Akita J, Mandai M, Honda Y, Takahashi M. Potential for neural regeneration after neurotoxic injury in the adult mammalian retina. Proceedings of the National Academy of Sciences of the United States of America. 2004; 101:13654–13659. [PubMed: 15353594]

Oswald M, Robison BD. Strain-specific alteration of zebrafish feeding behavior in response to aversive stimuli. Canadian journal of zoology. 2008; 86:1085–1094. [PubMed: 21379405]

Picker A, Brand M. Fgf signals from a novel signaling center determine axial patterning of the prospective neural retina. Development. 2005; 132:4951–4962. [PubMed: 16236770]

Pollak J, Wilken MS, Ueki Y, Cox KE, Sullivan JM, Taylor RJ, Levine EM, Reh TA. ASCL1 reprograms mouse Muller glia into neurogenic retinal progenitors. Development (Cambridge, England). 2013; 140:2619–2631.

Qin Z, Barthel LK, Raymond PA. Genetic evidence for shared mechanisms of epimorphic regeneration in zebrafish. Proceedings of the National Academy of Sciences of the United States of America. 2009; 106:9310–9315. [PubMed: 19474300]

Qin Z, Kidd AR 3rd, Thomas JL, Poss KD, Hyde DR, Raymond PA, Thummel R. FGF signaling regulates rod photoreceptor cell maintenance and regeneration in zebrafish. Experimental eye research. 2011; 93:726–734. [PubMed: 21945172]

Ramachandran R, Fausett BV, Goldman D. Ascl1a regulates Muller glia dedifferentiation and retinal regeneration through a Lin-28-dependent, let-7 microRNA signalling pathway. Nature cell biology. 2011a; 12:1101–1107.

Ramachandran R, Reifler A, Parent JM, Goldman D. Conditional gene expression and lineage tracing of tuba1a expressing cells during zebrafish development and retina regeneration. The Journal of comparative neurology. 2010; 518:4196–4212. [PubMed: 20878783]

Ramachandran R, Zhao XF, Goldman D. Ascl1a/Dkk/beta-catenin signaling pathway is necessary and glycogen synthase kinase-3beta inhibition is sufficient for zebrafish retina regeneration. Proceedings of the National Academy of Sciences of the United States of America. 2011b; 108:15858–15863. [PubMed: 21911394]

Ramachandran R, Zhao XF, Goldman D. Insm1a-mediated gene repression is essential for the formation and differentiation of Muller glia-derived progenitors in the injured retina. Nature cell biology. 2012; 14:1013–1023.

Raymond PA, Barthel LK, Bernardos RL, Perkowski JJ. Molecular characterization of retinal stem cells and their niches in adult zebrafish. BMC developmental biology. 2006; 6:36. [PubMed: 16872490]

Raymond PA, Reifler MJ, Rivlin PK. Regeneration of goldfish retina: rod precursors are a likely source of regenerated cells. J Neurobiol. 1988; 19:431–463. [PubMed: 3392530]

Reese BE, Galli-Resta L. The role of tangential dispersion in retinal mosaic formation. Prog Retin Eye Res. 2002; 21:153–168. [PubMed: 12062533]

Sapkota D, Wu F, Mu X. Focus on Molecules: Math5 and retinal ganglion cells. Experimental eye research. 2011; 93:796–797. [PubMed: 22019371]

Schindelin J, Arganda-Carreras I, Frise E, Kaynig V, Longair M, Pietzsch T, Preibisch S, Rueden C, Saalfeld S, Schmid B, Tinevez JY, White DJ, Hartenstein V, Eliceiri K, Tomancak P, Cardona A. Fiji: an open-source platform for biological-image analysis. Nature methods. 2012; 9:676–682. [PubMed: 22743772]

Sherpa T, Fimbel SM, Mallory DE, Maaswinkel H, Spritzer SD, Sand JA, Li L, Hyde DR, Stenkamp DL. Ganglion cell regeneration following whole-retina destruction in zebrafish. Developmental neurobiology. 2008; 68:166–181. [PubMed: 18000816]

Sherpa T, Hunter SS, Frey RA, Robison BD, Stenkamp DL. Retinal proliferation response in the buphthalmic zebrafish, bugeye. Experimental eye research. 2011 In press.

Shkumatava A, Fischer S, Muller F, Strahle U, Neumann CJ. Sonic hedgehog, secreted by amacrine cells, acts as a short-range signal to direct differentiation and lamination in the zebrafish retina. Development (Cambridge, England). 2004; 131:3849–3858.

Silver PH. Photopic spectral sensitivity of the neon tetra (Paracheirodon innesi (Myers)) found by the use of a dorsal light reaction. Vision Res. 1974; 14:329–334. [PubMed: 4830684]

Song WT, Zhang XY, Xia XB. Atoh7 promotes the differentiation of retinal stem cells derived from Muller cells into retinal ganglion cells by inhibiting Notch signaling. Stem cell research & therapy. 2013; 4:94. [PubMed: 23945288]

Spence JR, Madhavan M, Ewing JD, Jones DK, Lehman BM, Del Rio-Tsonis K. The hedgehog pathway is a modulator of retina regeneration. Development (Cambridge, England). 2004; 131:4607–4621.

Stacher Horndli C, Chien CB. Sonic hedgehog is indirectly required for intraretinal axon pathfinding by regulating chemokine expression in the optic stalk. Development (Cambridge, England). 2012; 139:2604–2613.

Stenkamp DL. The rod photoreceptor lineage of teleost fish. Progress in retinal and eye research. 2011; 30:395–404. [PubMed: 21742053]

Stenkamp DL, Cameron DA. Cellular pattern formation in the retina: retinal regeneration as a model system. Molecular vision. 2002; 8:280–293. [PubMed: 12181523]

Stenkamp DL, Frey RA, Prabhudesai SN, Raymond PA. Function for Hedgehog genes in zebrafish retinal development. Developmental biology. 2000; 220:238–252. [PubMed: 10753513]

Stenkamp DL, Powers MK, Carney LH, Cameron DA. Evidence for two distinct mechanisms of neurogenesis and cellular pattern formation in regenerated goldfish retinas. The Journal of comparative neurology. 2001; 431:363–381. [PubMed: 11223808]

Stenkamp DL, Satterfield R, Muhunthan K, Sherpa T, Vihtelic TS, Cameron D. Age-Related Cone Abnormalities in Zebrafish with Genetic Lesions in Sonic Hedgehog. Invest Ophthalmol Vis Sci. 2008a

Stenkamp DL, Satterfield R, Muhunthan K, Sherpa T, Vihtelic TS, Cameron DA. Age-related cone abnormalities in zebrafish with genetic lesions in sonic hedgehog. Investigative ophthalmology & visual science. 2008b; 49:4631–4640. [PubMed: 18502998]

Strahle U, Fischer N, Blader P. Expression and regulation of a netrin homologue in the zebrafish embryo. Mechanisms of development. 1997; 62:147–160. [PubMed: 9152007]

Stuermer CA. Trajectories of regenerating retinal axons in the goldfish tectum: II. Exploratory branches and growth cones on axons at early regeneration stages. The Journal of comparative neurology. 1988; 267:69–91. [PubMed: 3343393]

Thummel R, Enright JM, Kassen SC, Montgomery JE, Bailey TJ, Hyde DR. Pax6a and Pax6b are required at different points in neuronal progenitor cell proliferation during zebrafish photoreceptor regeneration. Experimental eye research. 2011; 90:572–582. [PubMed: 20152834]

Tulvatana W, Adamian M, Berson EL, Dryja TP. Photoreceptor rosettes in autosomal dominant retinitis pigmentosa with reduced penetrance. Arch Ophthalmol. 1999; 117:399–402. [PubMed: 10088824]

Udvadia AJ. 3.6 kb genomic sequence from Takifugu capable of promoting axon growth-associated gene expression in developing and regenerating zebrafish neurons. Gene Expr Patterns. 2008; 8:382–388. [PubMed: 18599366]

Ueki Y, Reh TA. EGF stimulates Muller glial proliferation via a BMP-dependent mechanism. Glia. 2013; 61:778–789. [PubMed: 23362023]

Veldman MB, Bemben MA, Thompson RC, Goldman D. Gene expression analysis of zebrafish retinal ganglion cells during optic nerve regeneration identifies KLF6a and KLF7a as important regulators of axon regeneration. Dev Biol. 2007; 312:596–612. [PubMed: 17949705]

Vihtelic TS, Hyde DR. Light-induced rod and cone cell death and regeneration in the adult albino zebrafish (Danio rerio) retina. Journal of neurobiology. 2000; 44:289–307. [PubMed: 10942883]

Vihtelic TS, Soverly JE, Kassen SC, Hyde DR. Retinal regional differences in photoreceptor cell death and regeneration in light-lesioned albino zebrafish. Experimental eye research. 2006; 82:558–575. [PubMed: 16199033]

Wallace VA, Raff MC. A role for Sonic hedgehog in axon-to-astrocyte signalling in the rodent optic nerve. Development. 1999; 126:2901–2909. [PubMed: 10357934]

Wan J, Ramachandran R, Goldman D. HB-EGF is necessary and sufficient for Muller glia dedifferentiation and retina regeneration. Developmental cell. 2012; 22:334–347. [PubMed: 22340497]

Wan J, Zheng H, Chen ZL, Xiao HL, Shen ZJ, Zhou GM. Preferential regeneration of photoreceptor from Muller glia after retinal degeneration in adult rat. Vision research. 2008; 48:223–234. [PubMed: 18155124]

Wang SW, Mu X, Bowers WJ, Kim DS, Plas DJ, Crair MC, Federoff HJ, Gan L, Klein WH. Brn3b/Brn3c double knockout mice reveal an unsuspected role for Brn3c in retinal ganglion cell axon outgrowth. Development. 2002a; 129:467–477. [PubMed: 11807038]

Wang YP, Dakubo G, Howley P, Campsall KD, Mazarolle CJ, Shiga SA, Lewis PM, McMahon AP, Wallace VA. Development of normal retinal organization depends on Sonic hedgehog signaling from ganglion cells. Nat Neurosci. 2002b; 5:831–832. [PubMed: 12195432]

Westerfield, M. The Zebrafish Book: A Guide for the Laboratory Use of Zebrafish (Danio rerio). University of Oregon Press; Eugene, OR: 2000.

Whitney IE, Raven MA, Ciobanu DC, Poche RA, Ding Q, Elshatory Y, Gan L, Williams RW, Reese BE. Genetic modulation of horizontal cell number in the mouse retina. Proceedings of the National Academy of Sciences of the United States of America. 2011; 108:9697–9702. [PubMed: 21576457]

Wu DM, Schneiderman T, Burgett J, Gokhale P, Barthel L, Raymond PA. Cones regenerate from retinal stem cells sequestered in the inner nuclear layer of adult goldfish retina. Invest Ophthalmol Vis Sci. 2001; 42:2115–2124. [PubMed: 11481280]

Yurco P, Cameron DA. Responses of Muller glia to retinal injury in adult zebrafish. Vision research. 2005; 45:991–1002. [PubMed: 15695184]

Zhang XM, Yang XJ. Regulation of retinal ganglion cell production by Sonic hedgehog. Development (Cambridge, England). 2001; 128:943–957.

Zhou H, Yoshioka T, Nathans J. Retina-derived POU-domain factor-1: a complex POU-domain gene implicated in the development of retinal ganglion and amacrine cells. J Neurosci. 1996; 16:2261–2274. [PubMed: 8601806]

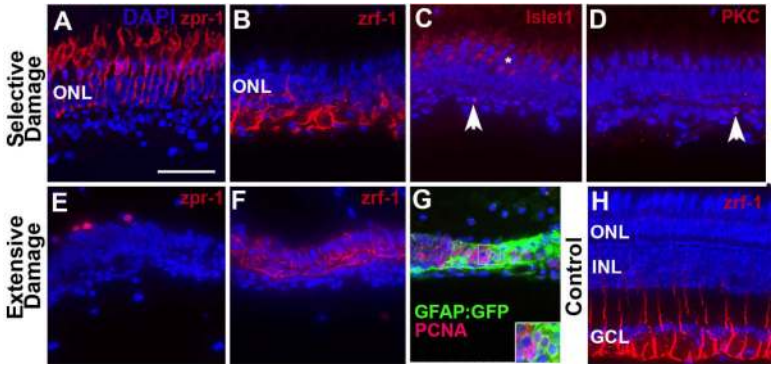

Figure 1.

Characterization of surviving retinal cells following selective or extensive damage. **A–D**. Retina was subjected to selective damage and processed for sectioning and indirect immunofluorescence three days after the ouabain injection. Cone photoreceptors (A; zpr-1+) appear uninjured; Müller glia (B; zrf-1+) are present but show unusual morphologies; rarely islet1+ cells (C; horizontal cells or debris, arrowhead) are present; and even more rarely PKCα+ cells (D; bipolar cells or debris, arrowhead) survive the injury. **E–F**. Retina was subjected to extensive damage and processed for sectioning and indirect immunofluorescence four days after the ouabain injection. Cone photoreceptor debris (E; zpr-1+) is present; Müller glia (F; zrf-1+) are present but show highly unusual morphologies. **G**. GFAP:GFP transgenic retina subjected to extensive damage and processed for confocal imaging of GFP, PCNA, and DAPI. Clusters of PCNA+/DAPI+ nuclei are surrounded by GFAP+ cytoplasm. **H**. Undamaged adult zebrafish retina labeled with zrf-1 to show normal morphological appearance of basal glial processes. Scale bar (applies to all) = 25 μm.

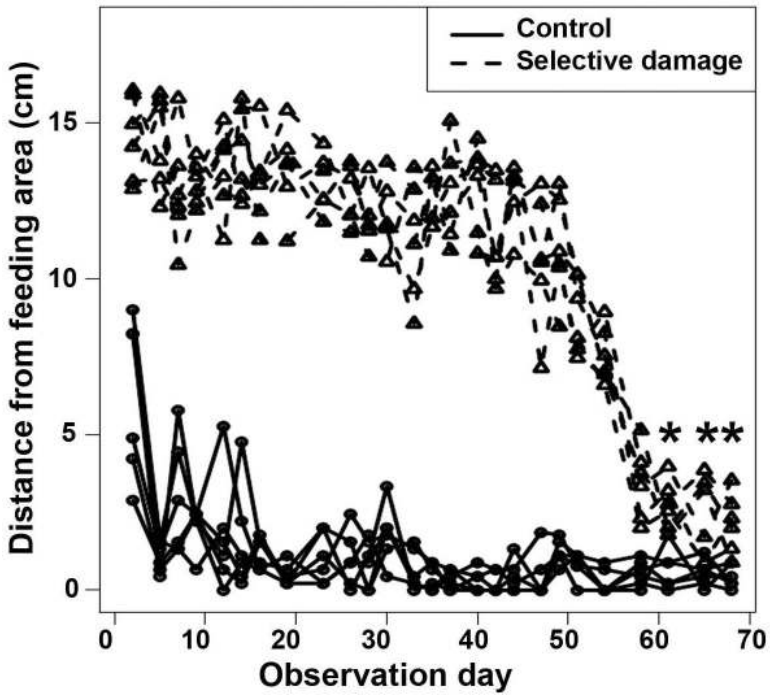

Figure 2.

Visual recovery following selective destruction of inner retinal neurons. Figure shows the positions of 14 month-old fish in the tank in response to a hand waved near the feeding area. Round symbols indicate positions of untreated control fish (near the feeding area), triangular symbols indicate positions of fish subjected to selective damage to inner retinal neurons. The positions of treated fish were significantly different from the positions of control fish until observation day 61 and beyond, indicating blindness followed by restoration of vision at 61 days ($p<0.05$; Simultaneous Tests for General Linear Hypotheses (Hothorn et al., 2008). In this figure, the asterisks (*) indicate the lack of significant difference between the two groups.

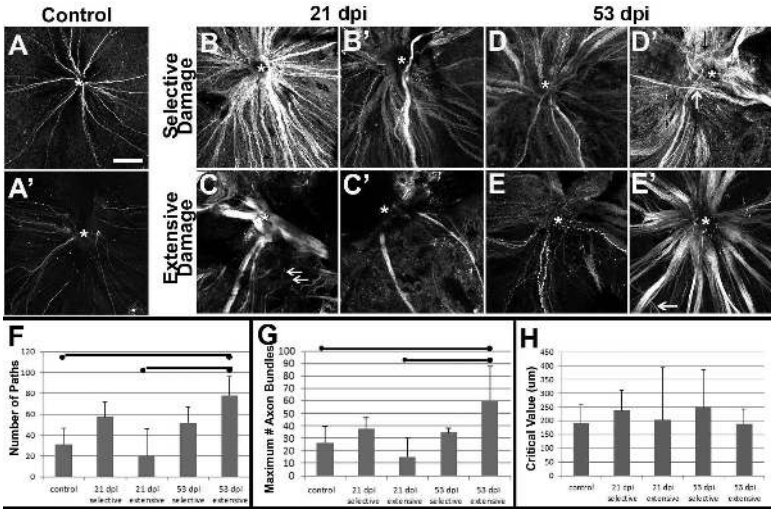

Figure 3.

Axon trajectories of growing retinal ganglion cells within regenerating retinas following selective vs. extensive lesion. **A**. Two examples of whole-mounted, *gap43:GFP* zebrafish retina showing a small number of GFP+, growing axon bundles originating from RGCs near the retinal margin and converging at the optic nerve head (ONH, marked by *). **B**. Two examples of whole-mounted, *gap43:GFP* zebrafish retina regenerating after a lesion selective to the inner retinal layers and processed at 21 dpi, showing numerous GFP+, growing axon bundles converging at the ONH. **C**. Two examples of whole-mounted, *gap43:GFP* retina regenerating after an extensive lesion and processed at 53 dpi, showing a small number of very thick and disorganized axon bundles (C) or very few moderately thick axon bundles (C'). Many thin bundles in C do not reach the ONH (arrows). **D**. Two examples of whole-mounted, *gap43:GFP* zebrafish retina regenerating after a selective lesion and processed at 53 dpi, the image in D' shows a mis-targeted axon bundle (white arrow), and some narrow, wandering axon bundles (black arrow). **E**. Two examples of whole-mounted, *gap43:GFP* retina regenerating after an extensive lesion and processed at 50 (E') or 53 (E) dpi, showing predominantly narrow (E) or thick (E') axon bundles. Most axon bundles converge at the ONH (*), while others show irregular trajectories (arrow). Scale bar in A (applies to all) = 100 μm. **F**. Number of axon bundle paths as detected by Sholl analysis (mean +/− S.D.), bars indicate statistical significance between groups (ANOVA with Bonferroni post-hoc analysis). **G**. Maximum number of axon bundles as detected by Sholl analysis (mean +/− S.D.), bars indicate statistical significance between groups (ANOVA with Bonferroni post-hoc analysis). **H**. Sholl critical values (distance at which maximum number of axon bundles were detected; mean +/− S.D.), no differences were statistically significant (ANOVA).

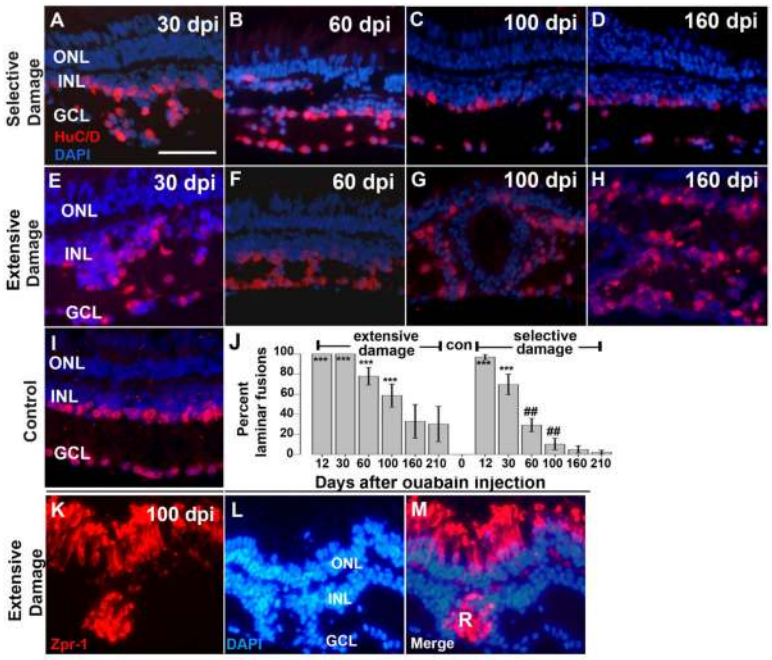

Figure 4.

Retinal lamination in regenerating retinas after selective or extensive retinal damage. **A–I**. Fixed, frozen retinal sections were immunolabeled with anti- HuC/D monoclonal antibody, to detect differentiated amacrine and ganglion cells, and mounted in the presence of the DAPI nuclear stain. Retinal lamination of regenerating retina after selective damage (A–D) and extensive damage (E–H), was assessed at 30 dpi (days post-injection; A,E), 60 dpi (B,F), 100dpi (C,G) and 160 dpi (D,H); examples of laminar fusions are indicated by white asterisks (*). Control section from a wild type retina is shown in (I). **J**. Barplot shows proportion of retinal sections showing laminar fusions (see Methods) following extensive or selective retinal damage as a function of recovery time; con=control (no laminar fusions). Asterisks (*) indicate significant differences from control (**, $p<0.01$; ***, $p<0.001$; two-sample Wilcoxon rank sum test) and the number signs (##) indicate significant differences between extensive and selective damage at the same recovery time ($p<0.01$; two-sample Wilcoxon rank sum test). **K–M**. Rosette formation in regenerating retina after extensive retinal damage. Fixed, frozen retinal sections were immunolabeled with the zpr-1 monoclonal antibody (K), to detect differentiated cone photoreceptors, and mounted in the presence of the DAPI nuclear stain (L; merged images shown in M). Photoreceptor rosettes (R) are present in retina 100 dpi (days post-injection). This experiment was carried out for selectively damaged retina, but rosettes were rarely observed (Table 2). Scale bar (applies to A-I and K-M) = 25 μm. ONL, outer nuclear layer; INL, inner nuclear layer; GCL, ganglion cell layer).

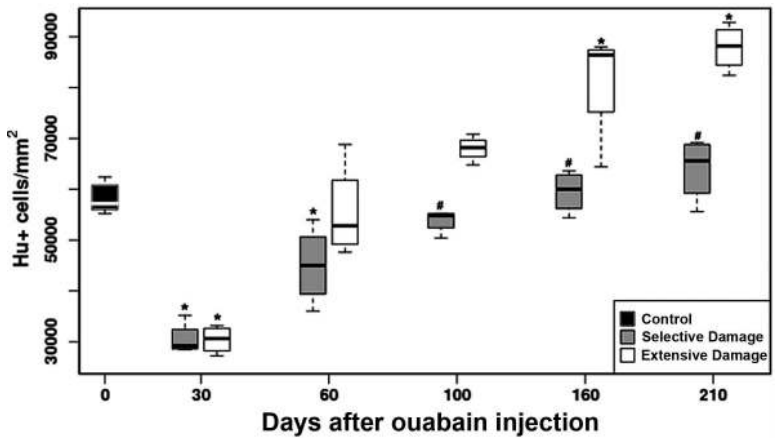

Figure 5.

Densities of HuC/D+ inner retinal neurons as a function of type of damage and recovery time. Asterisks (*) indicate significant differences from control densities ($p<0.05$) and number signs (#) indicate significant differences between selective vs. broad damage at the same sampling time [($p<0.05$) Simultaneous Tests for General Linear Hypotheses] (Hothorn et al., 2008).

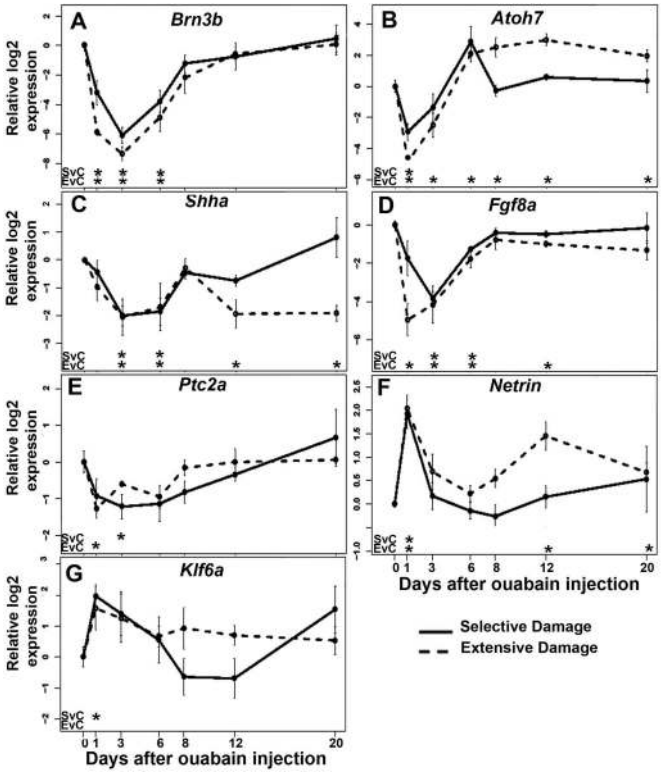

Figure 6.

Expression of genes related to ganglion cell development following selective or extensive retinal damage. Relative log2 expression of the genes *Brn3b* (A), *Ath5* (B), *Shha* (C), *Fgf8a* (D), *Ptc2a* (E), *Netrin* (F), and *KLF6a* (G) are presented as a function of recovery time. Significant differences ($p<0.01$; Welch two sample t-test) for selective damage vs. control (SvC), and for extensive damage vs. control (EvC) are shown under each plot. Y-axes in each panel are independently scaled because baseline expression of each gene was distinct.

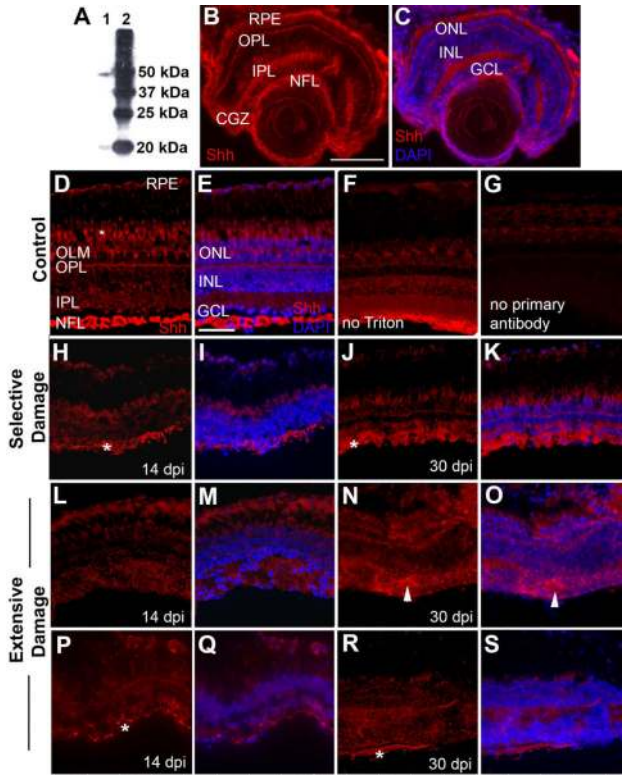

Figure 7.

Distribution of Hh protein in undamaged and regenerating zebrafish retinas. **A**. Western blotting results using the anti-Shh antibody from AnaSpec (AnaSpec, Fremont, CA; #55574). Lane 1, proteins derived from zebrafish embryos; lane 2, molecular size ladder. Proteins in lane 1 likely correspond to unprocessed (50kDa) and processed (20kDa) Hh protein. **B**. In a 4 day old larval zebrafish eye, anti-Shh antibody stains the retinal pigmented epithelium (RPE), the outer plexiform layer (OPL), the inner plexiform layer (IPL), the nerve fiber layer (NFL), and extracellular regions of the circumferential germinal zone (CGZ). **C**. Same as (B), but with DAPI staining to show locations of nuclear layers. OLM, outer limiting membrane; ONL, outer nuclear layer; INL, inner nuclear layer; GCL, ganglion cell layer. Scale bar in B (applies to **A–C**) = 100 μm. **D**. Undamaged adult zebrafish retina, showing Hh staining in the retinal pigmented epithelium (RPE), the inner and outer plexiform layers (IPL, OPL), the nerve fiber layer (NFL), and cone photoreceptor inner segments (*). **E**. Same as (D), but colabeled with DAPI to show positions of outer nuclear layer (ONL), inner nuclear layer (INL), and ganglion cell layer (GCL). **F**. Undamaged control retina, immunofluorescence performed in the absence of Triton X-100. **G**. Undamaged control retina, experiment performed in the absence of primary antibody. **H**. Retina subjected to selective damage of inner retinal layers, sampled at 14 dpi (days post-injury). The most intense staining corresponds to processes (asterisks) associated with an emerging NFL. RPE and photoreceptors are also stained. **I**. Same as (H) but colabeled with DAPI. **J**. Retina subjected to selective damage, sampled at 30 dpi. Staining pattern is similar to that of undamaged control retinas, with prominent staining of the NFL, although the retina remains histologically disorganized. **K**. Same as (J) but colabeled with DAPI. **L**.

Retina subjected to extensive damage of all retinal layers, sampled at 14 dpi. Regenerating plexiform layers are stained, but NFL staining is not evident. **M**. Same as (L) but colabeled with DAPI. **N**. Retina subjected to extensive damage, sampled at 30 dpi. Staining pattern includes regions of apparent ectopic Hh (arrowheads), associated with histological abnormalities. **O**. Same as (N) but colabeled with DAPI. **P**. Retina subjected to extensive damage, sampled at 14 dpi, view is of a rare region containing Hh staining at the vitreal surface (asterisk). **Q**. Same as (P) but colabeled with DAPI. **R**. Retina subjected to extensive damage, sampled at 30 dpi, view is of a rare region containing Hh staining at the vitreal surface (asterisk). **S**. Same as (R) but colabeled with DAPI. Scale bar in **E** (applies to D-N) = 25 μm.

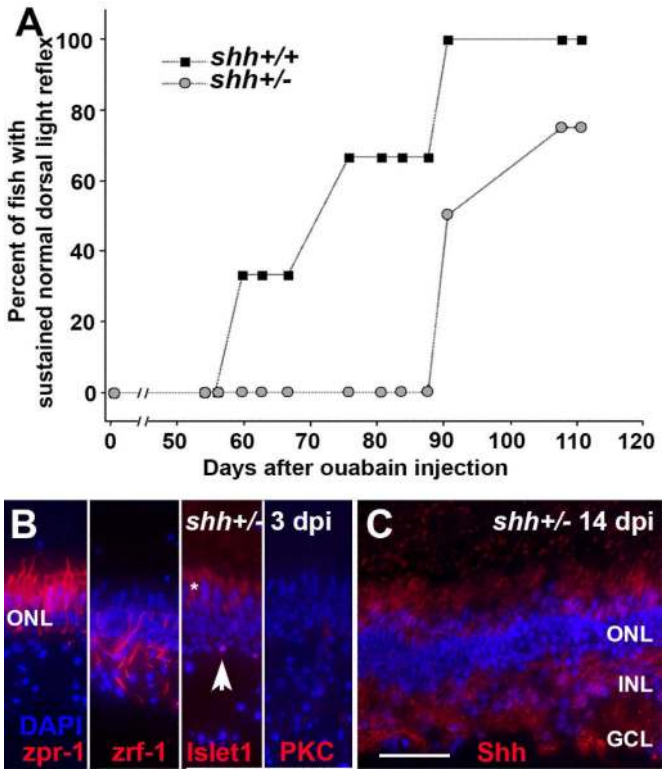

Figure 8.

A. Significantly delayed recovery of normal dorsal light reflex (DLR) following unilateral selective retinal lesion in *shha*^{t4}+/− zebrafish as compared to their *shha*+/+ siblings. Difference between groups, p=0.001 (logistic regression with repeated measures). **B.** Characterization of surviving retinal cells in *shha*^{t4}+/− retinas sampled at 3 dpi following selective damage. Cone photoreceptors (zpr-1+) are uninjured; Müller glia (zrf-1+) are present but show unusual morphologies; some horizontal cells (islet1+; arrowhead) are present but pyknotic; bipolar cells (PKC+) very rarely survive the injury. Asterisk (*) indicates autofluorescence of photoreceptor inner segments. **C.** Retinas of *shha*^{t4}+/− zebrafish subjected to selective damage display evidence of histological recovery, with widespread laminar fusions, at 14 dpi; compare to (Fimbel et al., 2007). Also at 14 dpi, the distribution of Hh protein (in red, with DAPI nuclear stain in blue) in *shha*^{t4}+/− retinas is diffuse (compare to Fig. 7). Scale bar in B (applies to B–C) = 25 μm.

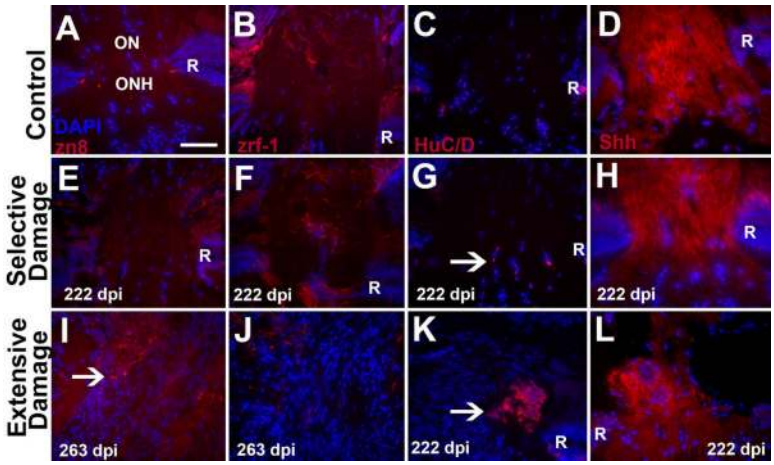

Figure 9.

Characterization of optic nerve heads (ONHs) at >200 days post ouabain lesion. **A.–D.** Control (undamaged) ONHs stained using markers (red) for growing axons (A, zn8), astrocytes (B, zrf-1), neurons (HuC/D), and Hh protein (Shh); all samples were counterstained with DAPI (blue). Optic nerves (ON) are at the top of each image; R, retina. **E.–H.** ONHs of eyes processed 222 days following selective damage to the inner retinal layers, showing very few growing axons (E, similar to control), the presence of astrocyte processes (F, though less organized than control), a small number of neurons (arrow in G, compare to none in control), and Hh protein associated with the ONH (H). **I.–L.** ONHs of eyes processed 222 (K,L) or 263 (I,J) days following extensive damage to all retinal neurons, showing numerous growing axons with irregular trajectories (arrow in I), very few astrocyte processes (J), clusters of ectopic neurons (arrow in I), and Hh protein distribution consistent with axon misrouting through ONH. Retinas are not visible in images I and J due to the very large sizes of these ONHs (Sherpa et al., 2008); images K and L show more eccentric samples in which retinas are visible. Scale bar in A (applies to all) = 50 μm.

Table 1

Primers for qRT-PCR.

Gene	Sequence
18s	5'-GAACGCCACTTGTCCCTCTA-3' and 5'-GTTGGTGGAGCGATTTGTCT-3'
Her4.2	5'-CCACTGAAACACACGCAAAC-3' and 5'-TCAGACTGGCATCGTGACTC-3'
Ath5	5'- TGCAAGAGAACGAAAGAGAGTGC- 3' and 5'-TTCCGAAGCCGGTCGAA - 3'
Brn3b	5'- AAAGTCGCACCGGGAGAAA-3' and 5'- TTCTCGGCCCCGTTGA -3'
fgf8a	5'- GCTCCAAAACCAGGCAACA -3' and 5'-CTTGGGCAACCTCTTCATGAA- 3'
shha	5' -GGTGTTCAGCGACTTCATCA – 3' and 5'-AACGGGTTCTTGCGTTTCTA- 3'
ptc-2A	5'-TGGCGCTAGCGTAGCTTTG- 3' and 5'- GGGCGGCCATAAAAAACG -3'
Netrin	5'- GTCAAAGACCGGGATGGAAA -3' and 5'- TGGTCCGGCTGTGTTGTG -3'
KLF6a	5'- GCAAGGAGCGATGAGCTAAC-3' and 5'- GCAAGGAGCGATGAGCTAAC-3'

Table 2

Presence of rosettes in regenerated retina following extensive vs. selective damage.

Sampling time	# Retinas with rosettes (# retinas analyzed)		Fisher exact test
	Extensive damage	Selective damage	
100 dpi	2 (4)	0 (5)	p=0.1667
160 dpi	4 (4)	1 (5)	p=0.0476
200 dpi	4 (4)	0 (8)	p=0.002
300 dpi	4 (4)	0 (4)	p=0.0286

Table 3

Summary of outcomes for extensive vs. selective retinal damage.

Criterion	Extensive damage	Selective damage	Reference
Cell types destroyed or spared	All neurons destroyed; spares Müller glia	Most neurons destroyed; spares photoreceptors and Müller glia	Present study (Fig. 1)
Müllerglia re-enter cell cycle	Yes	Yes	Present study (Fig. 1; Supplemental Fig. 1) Fimbel et al., 2007
Histological regeneration	12–14 dpi	12–14 dpi	Sherpa et al., 2008; Fimbel et al., 2007
Visual function	Returns at 98–100 dpi	Returns at 60–65 dpi	Sherpa et al., 2008; Present study (Fig. 2)
Optic nerve head diameter	Returns to normal at 100 dpi	Returns to normal at 60 dpi	Sherpa et al., 2008; Fimbel et al., 2007
RGC axon trajectories	Delayed and sporadic at 21 dpi; more complex patterns at 53 dpi	Converge upon ONH at 21 dpi and 53 dpi	Present study (Fig. 3; Supplemental Fig. 2)
Retinal lamination	Does not completely recover	Recovers	Present study (Fig. 4)
Rosette formation	Yes, after 100 dpi	Rarely	Present study (Fig. 4; Table 2)
Overproduction of HuC/D+ neurons	Yes	No	Present study (Fig. 5)
Shh expression and distribution	Reduced mRNA levels; Present in plexiform layers, diffuse elsewhere	RPE, plexiform layers, NFL	Present study (Figs. 6, 7)
Optic nerve head hypertrophy	Yes, after 100 dpi	No	Sherpa et al., 2008; Present study (Supplemental Fig. 3)
Optic nerve head abnormalities	Ectopic neurons and misrouted axons	None	Present study (Fig. 9)